Molecular Cell

Article

PLEKHS1 drives PI3Ks and remodels pathway homeostasis in PTEN-null prostate

Graphical abstract

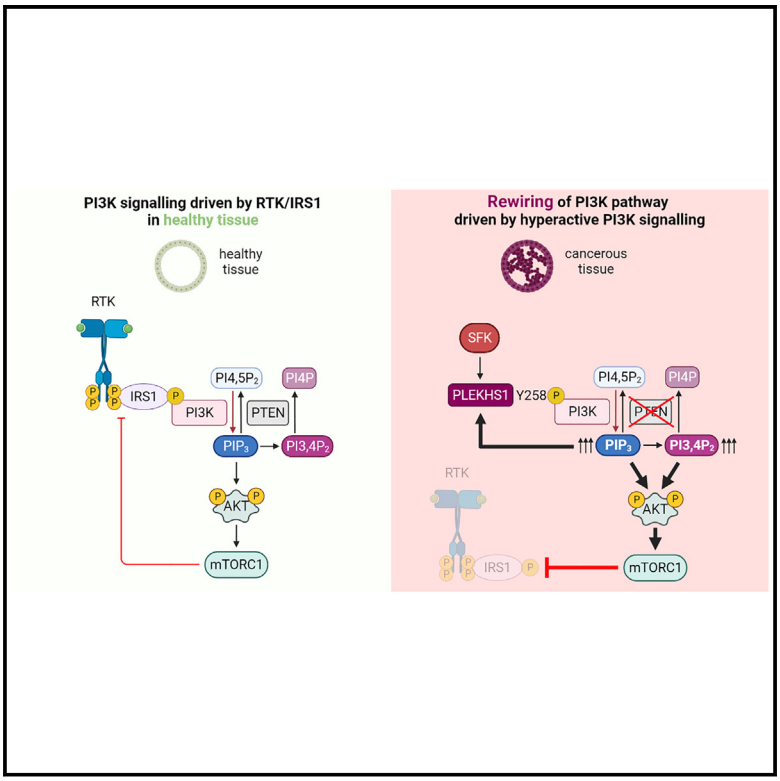

Authors

Tamara A.M. Chessa, Piotr Jung, Arqum Anwar, ..., Sabina Cosulich, Phillip T. Hawkins, Len R. Stephens

Correspondence

tamara.chessa@babraham.ac.uk (T.A.M.C.), len.stephens@babraham.ac.uk (L.R.S.)

In brief

The theory was simple. Loss of the PIP_3 phosphatase and negative regulator of the PI3K network, PTEN, caused a sustained increase in PIP_3/PI3K signaling and hence powered progression of many cancers. Recent work by Chessa et al. supersedes that model. PTEN KO results in massive pathway rewiring and a switch from receptor-dependent to cell-autonomous, self-reinforcing PI3K activation mechanisms.

Highlights

- In healthy tissue, IRS signaling and negative feedback set PI3K pathway activity
- Loss of PTEN leads to the adaptor PLEKHS1 becoming the main driver of PI3Ks
- The switch results in part from negative feedback suppressing IRS activation of PI3Ks
- PLEKHS1 evades negative feedback and is YXXM-phosphorylated by a PIP_3-dependent mechanism

Chessa et al., 2023, Molecular Cell *83*, 1–19
August 17, 2023
https://doi.org/10.1016/j.molcel.2023.07.015

CellPress

Please cite this article in press as: Chessa et al., PLEKHS1 drives PI3Ks and remodels pathway homeostasis in PTEN-null prostate, Molecular Cell (2023), https://doi.org/10.1016/j.molcel.2023.07.015

Molecular Cell

CellPress
OPEN ACCESS

Article

PLEKHS1 drives PI3Ks and remodels pathway homeostasis in PTEN-null prostate

Tamara A.M. Chessa,[1,*] Piotr Jung,[1,11] Arqum Anwar,[1,11] Sabine Suire,[1,11] Karen E. Anderson,[1] David Barneda,[1] Anna Kielkowska,[1] Barzan A. Sadiq,[1] Ieng Wai Lai,[1] Sergio Felisbino,[2] Daniel J. Turnham,[3] Helen B. Pearson,[3] Wayne A. Phillips,[4] Junko Sasaki,[5] Takehiko Sasaki,[5] David Oxley,[6] Dominik Spensberger,[7] Anne Segonds-Pichon,[8] Michael Wilson,[1] Simon Walker,[9] Hanneke Okkenhaug,[9] Sabina Cosulich,[10] Phillip T. Hawkins,[1,12] and Len R. Stephens[1,12,13,*]

[1]Signalling Programme, Babraham Institute, Cambridge CB22 3AT, UK
[2]Department of Structural and Functional Biology, São Paulo State University, Botucatu, SP CEP: 18618-689, Brazil
[3]European Cancer Stem Cell Research Institute, Cardiff University, Cardiff CF24 4HQ, UK
[4]Peter MacCallum Cancer Centre and Sir Peter MacCallum Department of Oncology, University of Melbourne, Melbourne, VIC, Australia
[5]Department of Biochemical Pathophysiology, Medical Research Institute, Tokyo Medical and Dental University, Tokyo 113-8510, Japan
[6]Mass Spectrometry Facility, Babraham Institute, Cambridge CB22 3AT, UK
[7]Gene Targeting Facility, Babraham Institute, Cambridge CB22 3AT, UK
[8]Bioinformatics, Babraham Institute, Cambridge CB22 3AT, UK
[9]Imaging Facility, Babraham Institute, Cambridge CB22 3AT, UK
[10]Projects Group, Oncology R&D, AstraZeneca, Cambridge, UK
[11]These authors contributed equally
[12]These authors contributed equally
[13]Lead contact
*Correspondence: tamara.chessa@babraham.ac.uk (T.A.M.C.), len.stephens@babraham.ac.uk (L.R.S.)
https://doi.org/10.1016/j.molcel.2023.07.015

SUMMARY

The PIP_3/PI3K network is a central regulator of metabolism and is frequently activated in cancer, commonly by loss of the PIP_3/$PI(3,4)P_2$ phosphatase, PTEN. Despite huge research investment, the drivers of the PI3K network in normal tissues and how they adapt to overactivation are unclear. We find that in healthy mouse prostate PI3K activity is driven by RTK/IRS signaling and constrained by pathway feedback. In the absence of PTEN, the network is dramatically remodeled. A poorly understood YXXM- and PIP_3/$PI(3,4)P_2$-binding PH domain-containing adaptor, PLEKHS1, became the dominant activator and was required to sustain PIP_3, AKT phosphorylation, and growth in PTEN-null prostate. This was because PLEKHS1 evaded pathway-feedback and experienced enhanced PI3K- and Src-family kinase-dependent phosphorylation of Y^{258}XXM, eliciting PI3K activation. *hPLEKHS1* mRNA and activating Y^{419} phosphorylation of hSrc correlated with PI3K pathway activity in human prostate cancers. We propose that in PTEN-null cells receptor-independent, Src-dependent tyrosine phosphorylation of PLEKHS1 creates positive feedback that escapes homeostasis, drives PIP_3 signaling, and supports tumor progression.

INTRODUCTION

The PIP_3 network is built around the ability of class I PI3Ks (phosphoinositide 3-kinases) to be activated by diverse signals and accelerate synthesis of the 2nd messengers PIP_3 (phosphatidylinositol (3,4,5)-trisphosphate) and its metabolite, $PI(3,4)P_2$. PIP_3 and $PI(3,4)P_2$ are capable of driving further signaling via PIP_3/$PI(3,4)P_2$-binding effector proteins, ultimately shaping many facets of cell biology and metabolism that support survival and growth.[1] PIP_3 and $PI(3,4)P_2$ can both be dephosphorylated by the 3-phosphatase, PTEN, and PIP_3 can additionally be dephosphorylated by SHIP-(1 and 2) 5-phosphatases,[2] to terminate signaling.[3,4] Many cancers harness mutations that drive the activity of the PIP_3 network, including loss of PTEN activity,[5–8] mutations in PI3K subunits (e.g., H1047R-p110α),[9] and in some cases mutations in other pathways that stimulate the pathway indirectly (e.g., SPOP in prostate cancer[10]), and this has driven huge investment in understanding and targeting the pathway.[1,11]

Class IA PI3Ks are heterodimers of a p85-family regulatory subunit (p85α, p85β, or p55γ, which contain SH2 domains) and a p110-family catalytic subunit (p110α, p110β, or p110δ). Both subunits are involved in the reception of diverse inputs. Signals from activated receptor tyrosine kinases (RTKs), in the form of tyrosine-phosphorylated YXXM motifs found in either the RTKs themselves (e.g., PDGFRβ) or closely associated adaptors (e.g., IRS or GAB family) can bind to the p85-SH2 domains and

Please cite this article in press as: Chessa et al., PLEKHS1 drives PI3Ks and remodels pathway homeostasis in PTEN-null prostate, Molecular Cell (2023), https://doi.org/10.1016/j.molcel.2023.07.015

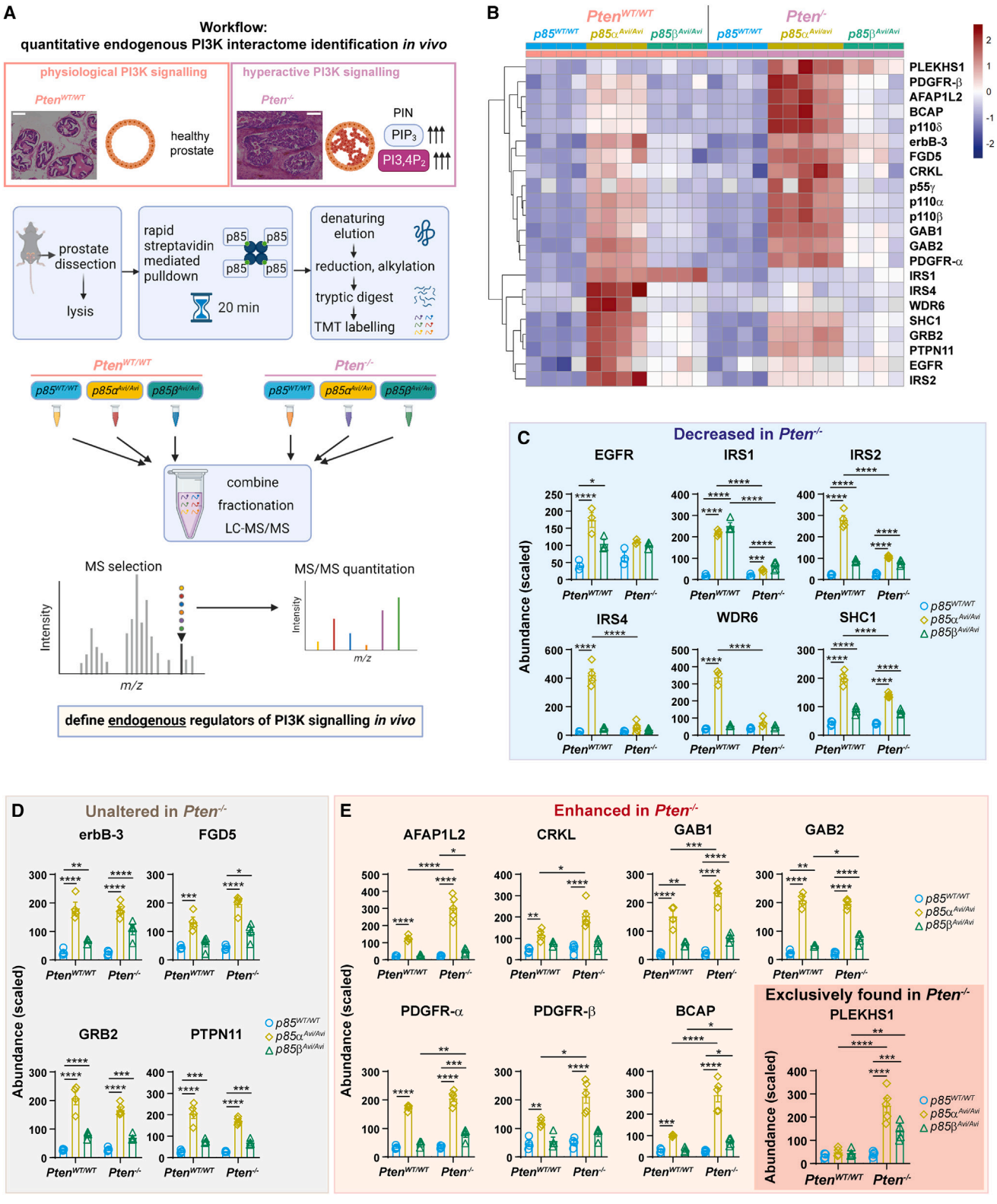

(legend on next page)

Please cite this article in press as: Chessa et al., PLEKHS1 drives PI3Ks and remodels pathway homeostasis in PTEN-null prostate, Molecular Cell (2023), https://doi.org/10.1016/j.molcel.2023.07.015

activate the catalytic subunit's kinase domain through a web of allosteric interactions that can be hijacked by PI3K oncomutants.[12]

Src-family tyrosine kinases (SFKs) can integrate a wide range of inputs (including FAK and the Src-like PTK6[13]). Activation by different mechanisms, including ROS/H_2O_2-mediated sulfenylation of two exposed cysteines[14] and loss of PTEN (as PTEN can dephosphorylate and inactivate PTK6[15]), ultimately switch SFKs from a closed inactive to an open active, Y^{419}-phosphorylated conformation (Y^{419} in human Src). Peptide sequences neighboring tyrosine residues are important determinants of substrate selection by tyrosine kinases;[16,17] however, the major factor governing SFK substrate selection *in vivo* is co-localization via SFK-SH3 and/or -SH2 domain interactions.[17–19] Very few SFK substrates are phosphorylated within YXXM motifs, and in most cases SFKs activate PI3Ks indirectly via phosphorylation of other kinases or, rarely, at non-YXXM sites.[20,21]

Use of PI3K pathway inhibitors in cancers, or transformed cell lines, with mutations leading to elevated PI3K network activity has revealed that there is feedback from active mTORC1: firstly, via $p70^{S6K}$ and/or Grb10, which leads to suppression of the expression and phosphorylation of key RTKs and their adaptors (e.g., IRS); and secondly, via 4E-BP1, which leads to increased accumulation of PTEN.[22–26]

Drivers of the PI3K pathway in cancer have been identified by antibody-directed p85 pulldowns followed by immunoblotting for candidates. These studies repeatedly identified molecules like ERBB3, GAB1/2, PDGFRβ, and IRS-1 proteins as key[27–31] (in one case using proteomics to come to a similar conclusion[32]). The primary physiological molecular activators of class IA PI3Ks, however, remain poorly understood; consequently, important questions about whether or how physiological PI3K networks adapt or remodel in the face of sustained perturbations also remain unanswered.

We set out to systematically search for direct activators of the PI3K pathway in both normal mouse prostate and prostate in which the pathway had been chronically activated by loss of PTEN, using mice expressing endogenous p85α and p85β that are fully biotinylated and can be efficiently isolated with streptavidin-based tools.[33,34] Conditional deletion of PTEN in mouse prostate epithelium was achieved with a well-validated model ($Pten^{loxP/loxP}$ × $PbCre4^{+}$[35,36]) that leads to elevated PIP_3/PI(3,4)P_2, hyperplasia progressing to high-grade PIN from 3 to 7 months, with invasive adenocarcinoma emerging from 12 months.[37]

RESULTS

The endogenous p85-PI3K interactome is dramatically remodeled upon loss of PTEN *in vivo*

We aimed to define and semi-quantify the proteins associated with p85α and p85β PI3K complexes in wild-type (WT) and PTEN-knockout (KO) mouse prostate by proteomic analysis of streptavidin pulldowns and use of TMT labelling to barcode, multiplex, and compare the relative recovery of proteins between control pulldowns (e.g., $p85\alpha^{WT/WT}$ × $mBirA^{+/-}$) and specific pulldowns (e.g., $p85\alpha^{Avi/Avi}$ × $mBirA^{+/-}$). The workflow is summarized in Figures 1A and S1A (note: all mice express mBirA, but this is omitted from Figure 1A for clarity). The results showed that the presence of Avi-tags on endogenous p85s had no effect on their expression (Figure S1B) nor on PI3K activity as readout by PIP_3 accumulation in either WT or PTEN-KO prostate (Figure S1E) and that the protocol had worked effectively with efficient pulldown and specific recovery of p85α-Avi and p85β-Avi and associated p110s (Figures S1B–S1D). Twenty-four proteins were identified that were significantly recovered in pulldowns from $p85\alpha^{Avi/Avi}$ or $p85\beta^{Avi/Avi}$ compared to $p85^{WT/WT}$ prostate (Figure 1B). When plotted to show the relative moles of the associated proteins to be compared on a common scale (Figure S1F), then in WT prostate, IRS1 is the likely primary driver of the PIP_3 network. In PTEN-null tissue, the proteins recovered with p85s were changed entirely. IRS proteins were much reduced, with smaller but significant reductions in recovery of EGFR and SHC (Figures 1B and 1C); some interactors were unchanged (Figures 1B and 1D), while several increased substantially (Figures 1B and 1E).

Ranking the YXXM-containing adaptors according to their fold increase in PTEN-null compared to WT prostate identified PLEKHS1 (pleckstrin homology domain containing S1), a poorly understood GAB-related adaptor, as the most increased (Figures 1B, 1E, and S1H). PLEKHS1 and several other key interactors were also identified in p85 pulldowns from PTEN-KO and WT prostate by immunoblotting (Figure S1G; note: murine and hPLEKHS1 run anomalously during SDS-PAGE; the predicted sizes of their longest transcripts are 53–55 kDa, but they run with a mobility indicative of 70 kDa; see legend to Figure S1G).

IRS- but not PLEKHS1-mediated pathway activation is sensitive to pathway feedback

To investigate whether any of these changed associations was dependent on acute PI3K activity, mice were dosed with

Figure 1. The p85 interactome is dramatically rewired in PTEN-null prostate

Figure360▷ For a Figure360 author presentation of this figure, see https://doi.org/10.1016/j.molcel.2023.07.015.

(A) Methodology for identification of p85α and p85β interactors in $Pten^{WT/WT}$ and $Pten^{-/-}$ prostates (12 weeks). Scale bar, 100 μm.

(B) Proteins that were detected in n ≥ 3 biological replicates per genotype, and significantly more enriched in $p85\alpha$ or $\beta^{Avi/Avi}$ pulldowns compared to $p85^{WT/WT}$ pulldowns, were defined as specific p85 interactors. Multiple two-sided unpaired t tests (Holm correction) were performed. A stringent significance threshold ($p < 0.01$) was applied to identify proteins with increased detection above $p85^{WT/WT}$ controls, and specific interactors are visualized in a heatmap (clustering on *Z* scores of row-normalized values).

(C) Data are scaled abundances of p85 interactors that were decreased in $Pten^{-/-}$ tissue (n = 4–5 biological replicates per genotype, as indicated in B and as described in the STAR Methods and the legend to Figures S1C and S1D. Data for PI3K subunits is shown in Figures S1C and S1D). Statistics: two-way ANOVA with Holm-Šídák's multiple comparisons test. Adjusted p value summaries <0.05 are indicated.

(D) As above, except the data are scaled abundances of p85 interactors that were unchanged in $Pten^{-/-}$ tissue.

(E) As above, except the data are scaled abundances of p85 interactors that were increased in $Pten^{-/-}$ tissue. See also Figures S1, S2, and S6.

Please cite this article in press as: Chessa et al., PLEKHS1 drives PI3Ks and remodels pathway homeostasis in PTEN-null prostate, Molecular Cell (2023), https://doi.org/10.1016/j.molcel.2023.07.015

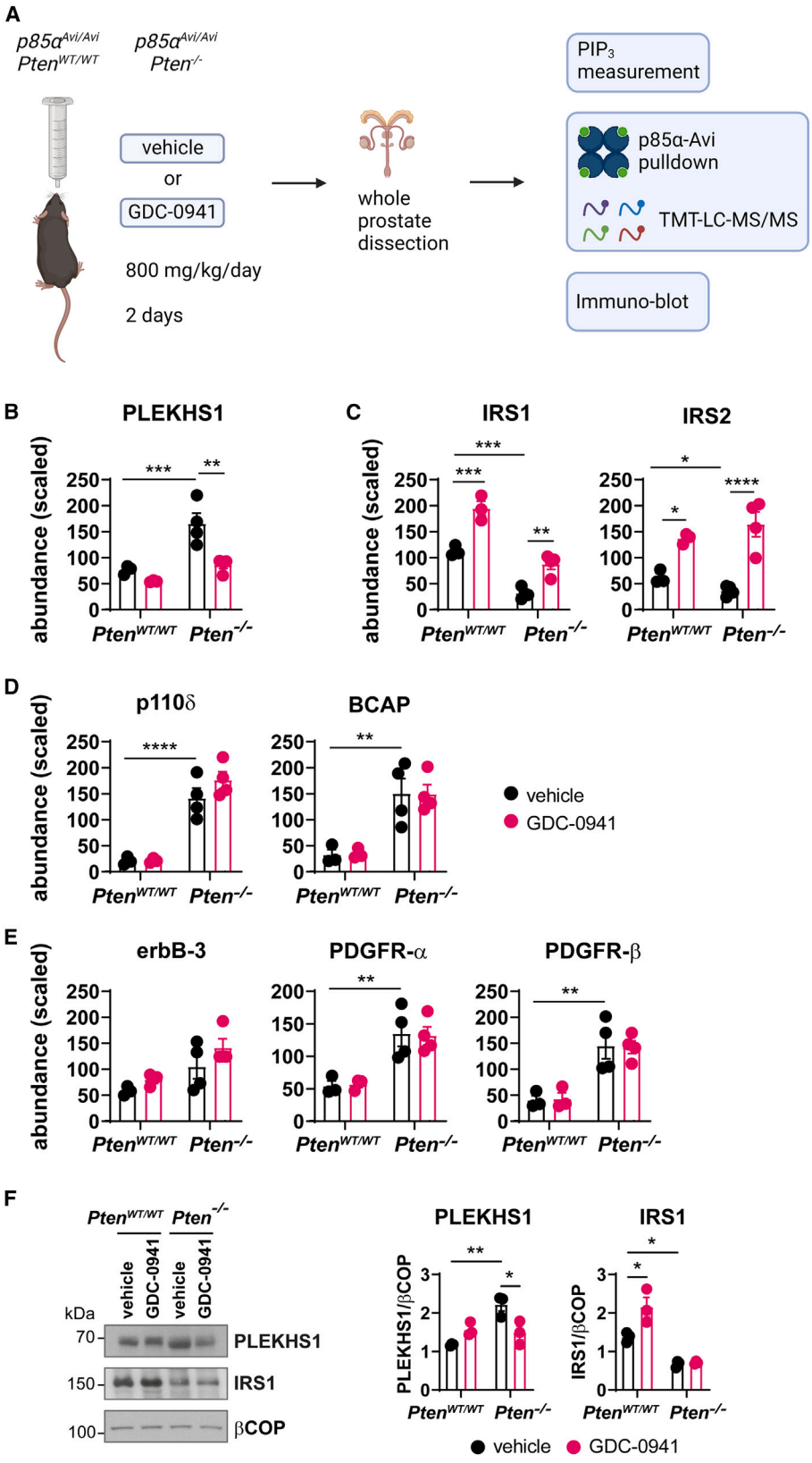

(legend on next page)

Please cite this article in press as: Chessa et al., PLEKHS1 drives PI3Ks and remodels pathway homeostasis in PTEN-null prostate, Molecular Cell (2023), https://doi.org/10.1016/j.molcel.2023.07.015

pan-class I PI3K inhibitor GDC-0941 (pictilisib[38]) (Figure 2A). The inhibitor reduced PIP_3 levels and AKT phosphorylation in the prostate, as expected (Figures S2A and S2C). This treatment regime had no effect on the recovery of most p85 interactors (Figures 2D, 2E, and S2B); however, recovery of IRS1 and IRS2 from both WT and PTEN-KO prostate was significantly increased (Figure 2C). In contrast, PI3K inhibition caused a decrease in PLEKHS1 recovery with p85s (Figure 2B).

To understand these changes in p85 interactomes, we examined published data measuring the mRNAs of these interactors in healthy or PTEN-KO mouse prostate (NCBI GEO: GSE94574,[37] comparing normal and PIN) and measured their abundance in prostate lysates. This revealed that the changes in p85 interactome upon loss of PTEN were very unlikely to be driven by changed expression, with the exception of the IRS family, where the levels of their mRNA and protein were substantially and significantly reduced in PTEN-KO prostate (Figures 2F, S2C, and S2D). In contrast, there was a small decrease in *Plekhs1* mRNA (Figure S2D) and a significant increase in PLEKHS1 protein in the absence of PTEN, with the latter reduced by PI3K inhibitors (Figures 2F and S2C).

Collectively, the results in Figures 1 and 2 are consistent with PI3K pathway feedback being active in healthy prostate. In PTEN-KO prostate tissue, that feedback intensified and further suppressed expression of IRS proteins (and WDR6, a known IRS4 interactor) and thus their ability to interact with p85s. The outcome is that IRS proteins become dramatically reduced and relatively minor drivers of the PI3K pathway in PTEN-KO prostate (Figure S1F).

Public datasets show that m*Plekhs1* mRNA is differentially expressed in a small number of tissues, including prostate, and we have confirmed that PLEKHS1 protein is expressed in mouse prostate (see below). To understand which cell types expressed PLEKHS1, we dissociated mouse prostate tissue and sorted into basal-epithelial, luminal-epithelial, and residual (including stromal and immune) cell bins and measured PLEKHS1 by immunoblotting. The large majority of PLEKHS1 was detected in epithelial cells in both WT and PTEN-KO prostate and was significantly enriched in luminal cells (Figures S3A and S3B). Importantly, the expression of PLEKHS1 was the same in luminal cells purified from PTEN-KO or WT prostate, suggesting that the increase in PLEKHS1 expression in PTEN-KO prostate resulted from an increase in the relative size of the luminal cell compartment (Figures S3A and S3B) and not an increase in its concentration in luminal cells. These results suggest that, in contrast to IRS proteins, PLEKHS1 is not subject to pathway feedback and that its increased association with p85s in PTEN-KO tissue is not a result of a dramatic change in its expression.

A subset of p85 interactors that are increased in PTEN-null prostate are a result of immune infiltration

Two p85 interactors that were increased in PTEN-KO prostate, BCAP/PIK3AP and p110δ, are differentially expressed in immune cells, particularly macrophages (Figures 1B, S2E, and S2F). Furthermore, the recovery of CSF1R in p85-Avi pulldowns was greater from PTEN-null compared to control prostate, although these data were not statistically significant because CSF1R peptides were detected in only 2 of 5 samples (Figure S2E). This may reflect infiltration of myeloid-derived suppressor cells, with active CSF1R/BCAP/PI3Kδ signaling, into the hyperplasic tissue, consistent with the activated immune-phenotype of the $Pten^{loxP/loxP} \times PbCre4^{+}$ model.[39] Interestingly, the recovery of these interactors with p85s was unchanged by PI3K inhibition (Figure 2D), suggesting that neither the assembly of these signaling complexes nor the infiltration of the relevant immune cells into the PTEN-KO prostate was acutely dependent on PI3K activity.

PLEKHS1 can be phosphorylated by Src-family kinases on Y^{258}XXM, can bind and activate PI3K signaling, and contains a PH domain that can bind $PI(3,4)P_2$ and PIP_3

Previous work has shown that the YXXM motif in hPLEKHS1 (equivalent to Y^{258} in the mouse; Figure 3A) can be tyrosine phosphorylated by a variety of non-receptor tyrosine kinases and bind to the C-terminal SH2 domain of p55γ in heterologous expression systems.[40] Furthering this work, we used HeLa and LNCaP cells (a human, PTEN-null prostate cancer cell line) to demonstrate that heterologous Y^{527}F-c-src but not K^{295}R-c-src (constitutively active and inactive alleles, respectively; Figure 3B) drives both phosphorylation of Y^{258} in heterologous mPLEKHS1 and Y^{258}-mPLEKHS1-dependent binding of mPLEKHS1 to endogenous p55γ and p85 subunits. In LNCaP cells, over-expression of mPLEKHS1 alone increased PIP_3 levels in a manner disrupted by Y^{258}F mutation of PLEKHS1, suggesting that endogenous kinases had phosphorylated Y^{258}-PLEKHS1 and driven activation of class IA PI3K signaling (Figure 3C).

PLEKHS1 contains a PH domain, with key similarities to PIP_3-binding PH domains (Figure 3A). We tested whether full-length PLEKHS1 or its isolated PH domain could selectively bind phosphoinositides presented in either protein-lipid overlay assays or sucrose-loaded liposomes with a plasma membrane-like mix of phospholipids. Both constructs selectively bound PIP_3 and $PI(3,4)P_2$ with similar apparent affinity (Figures 3D–3G).

Pulldown of endogenous PLEKHS1 shows that interactions with PI3Ks and 14:3:3 proteins are increased in PTEN-null tissue

To independently test the idea that PLEKHS1 can interact with p85s and that this is augmented in PTEN-null prostate and to

Figure 2. IRS- but not PLEKHS1-mediated pathway activation is sensitive to pathway feedback

(A) Diagram of dosing schedule of $p85\alpha^{Avi/Avi} \times Pten^{WT/WT}$ and $p85\alpha^{Avi/Avi} \times Pten^{-/-}$ mice with pan-class I PI3K inhibitor GDC-0941 and experimental workflow.
(B–E) Targeted TMT-LC-MS/MS analysis of the indicated proteins in $p85\alpha^{Avi/Avi} \times Pten^{WT/WT}$ and $p85\alpha^{Avi/Avi} \times Pten^{-/-}$ prostates (24–32 weeks), treated with vehicle or GDC-0941. Data are mean ± SEM for n = 3–4 biological replicates per genotype/condition, as described in the legend to Figure S2B.
(F) PLEKHS1 (G17) and IRS1 (2382) immunoblots of total lysates from $p85\alpha^{Avi/Avi} \times Pten^{WT/WT}$ and $p85\alpha^{Avi/Avi} \times Pten^{-/-}$ prostates, treated with vehicle or GDC-0941 (20 μg total protein/lane). Data are mean ± SEM of 3 biological replicates per genotype/condition, run and analyzed as a single cohort. A representative blot is shown, and the complete dataset is shown in Figure S2C. Statistics of (B)–(F): two-way ANOVA with Holm-Šídák's multiple comparisons test. See also Figure S2.

Please cite this article in press as: Chessa et al., PLEKHS1 drives PI3Ks and remodels pathway homeostasis in PTEN-null prostate, Molecular Cell (2023), https://doi.org/10.1016/j.molcel.2023.07.015

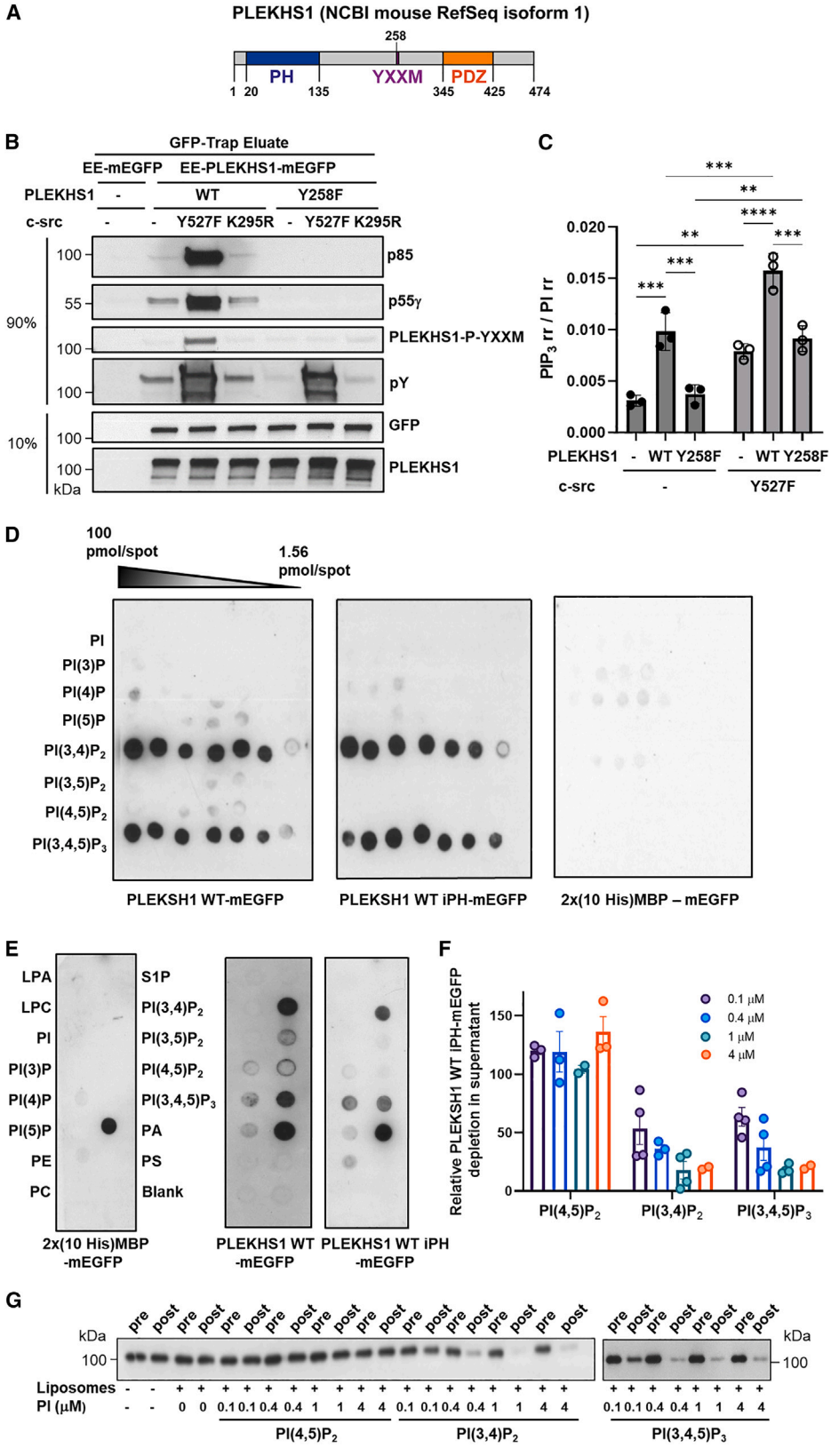

(legend on next page)

Please cite this article in press as: Chessa et al., PLEKHS1 drives PI3Ks and remodels pathway homeostasis in PTEN-null prostate, Molecular Cell (2023), https://doi.org/10.1016/j.molcel.2023.07.015

improve our ability to quantify PLEKHS1 and its phosphorylation *in vivo*, we generated mouse strains in which an Avi-tag was knocked in to the 3′-end of the endogenous *Plekhs1* locus (Figure S3C). *Plekhs1*$^{Avi/Avi}$ mice were viable with no overt or prostate-growth/morphology phenotypes. Expression of PLEKHS1 was unchanged in *Plekhs1*$^{Avi/Avi}$ prostate, and PLEKHS1-Avi could be completely, specifically depleted from lysates of m*BirA*$^{+/-}$ mice with streptavidin beads (Figure S3D). Immunoblotting with both anti-PLEKHS1 and anti-Avi antibodies (Figure S3E and S3F) revealed that PLEKHS1 is differentially expressed with relatively high levels in prostate, oviduct, and uterus and undetectable levels in the other tissues we sampled, broadly confirming the published tissue distribution of *mPlekhs1* mRNAs. *Plekhs1*$^{Avi/Avi}$ mice were interbred with *mBirA*$^{+/-}$, *Pten*$^{loxP/loxP}$, and *PbCre4*$^{+}$ mice to yield the relevant genotypes for experiments. Streptavidin pulldowns revealed a dramatic increase in recovery of PI3K subunits and 14:3:3 proteins in PTEN-KO tissue (Figures 4B and 4C), the former confirming results with p85α-Avi and p85β-Avi-expressing prostate. STRING and gene ontology analysis of PLEKHS1-interacting proteins whose recovery was significantly increased from PTEN-null compared to WT prostate did not implicate RTKs or their proximal adaptors (Figure 4A), unlike similar analyses of public, experimental data for mGAB or mIRS proteins (Figures 4E and 4F). These data suggest that in PTEN-null tissue PLEKHS1 is, at most, weakly regulated by RTKs.

Y^{258}XXM-PLEKHS1 is phosphorylated in a PI3K- and Src-family kinase-dependent fashion

Phospho-proteomic analysis of PLEKHS1-Avi pulldowns detected phosphorylation of Y^{258}-PLEKHS1, which was significantly increased in PTEN-KO prostate, and a further fifteen serine and five threonine residues that were unambiguously phosphorylated *in vivo* (Figure S4A). Pulldowns with anti-phospho-tyrosine antibodies followed by immunoblotting with anti-PLEKHS1 antibodies showed that there was an increase in total tyrosine phosphorylation of PLEKHS1 in PTEN-KO prostate (Figure S4B). In contrast, there was a decrease in pY-IRS1 in PTEN-KO prostate (Figure S4C). Immunoblotting PLEKHS1-Avi pulldowns with the anti-phospho-Y^{258}-PLEKHS1 antibody (validated in Figure 3B) revealed that phosphorylation of Y^{258}-PLEKHS1 was increased in PTEN-KO prostate, and this was significantly reduced in mice treated with PI3K inhibitor (Figure 5A). Further, treatment with PI3K inhibitor reduced recovery of associated p85α and p55γ (Figure 5A). Taken together, these results show that phosphorylation of Y^{258}-PLEKHS1 is increased in PTEN-KO tissue and sensitive to PI3K inhibitors. The ability of the PH domain of PLEKHS1 to bind PIP_3 and $PI(3,4)P_2$ offers a simple molecular explanation: the dramatically increased levels of those lipids in PTEN-KO prostate led to a redistribution of PLEKHS1 that is required for phosphorylation.

We used LNCaPs to address some mechanistic questions. In Figure 3 we showed that when *mPlekhs1*-eGFP was co-expressed with active c-src in LNCaP cells it was phosphorylated on Y^{258} and associated with endogenous p55γ. These events were inhibited by a PI3K inhibitor (Figure 5B). In contrast, a *mPlekhs1* construct lacking a PH domain (Δ1-135) showed relatively reduced phosphorylation of its YXXM motif and binding of p55γ, and both of those events were insensitive to PI3K inhibitors (Figure 5B).

Those results showed that the PH domain was required for the PI3K sensitivity of PLEKHS1 and suggest that binding of PI3K-generated lipids to the PH domain of PLEKHS1 enables heterologous c-src-mediated phosphorylation of Y^{258}XXM and association with the SH2 domains of the regulatory subunits of PI3Ks.

When mPLEKHS1-eGFP was expressed in the absence of heterologous Y527F-c-src it was still possible to detect clear binding of p55γ (Figure 3B). This binding of p55γ was unaffected by overnight serum starvation, suggesting it was not driven by serum-derived factors but reduced by a partially selective inhibitor of Src-family kinases (Figure 5C). We used it as a readout of endogenous phosphorylation of Y^{258}-PLEKHS1 and found that inhibitors that target SFKs, but not FAK-, BTK-, EGFR-, and EGFR/Her2-selective inhibitors, reduced binding of p55γ (Figure 5D). These results demonstrate endogenous SFKs can phosphorylate Y^{258}-mPLEKHS1 in LNCaP cells.

The expression and activity of SFKs in mouse prostate were substantially increased upon deletion of PTEN but insensitive to PI3K inhibitors (Figure S2C). These results strengthen the case that SFKs are responsible for phosphorylation of Y^{258}-PLEKHS1 in PTEN-KO prostate. They also suggest it is unlikely that the sensitivity of Y^{258}-PLEKHS1 phosphorylation to

Figure 3. PLEKHS1 can be phosphorylated by Src-family kinases on Y^{258}XXM and bind and activate PI3K signaling and contains a PH domain that can bind $PI(3,4)P_2$ and PIP_3

(A) Domain structure of the canonical sequence of mouse PLEKHS1 (NCBI RefSeq isoform 1).

(B) LNCaP cells were transfected with tagged m*Plekhs1* (WT-EE-*Plekhs1*-mEGFP [WT] or Y258F-EE-*Plekhs1*-mEGFP [Y258F]) or vector alone (EE-mEGFP), with or without constitutively active c-src (Y527F) or kinase-dead c-src (K295R). Lysates were prepared and subjected to GFP-trap pulldown, and the eluates were immunoblotted as indicated to assay PLEKHS1 interaction with PI3K regulatory subunits (p85, p55γ) and PLEKHS1 Tyr phosphorylation (total or pY^{258}XXM) with GFP and PLEKHS1 as input controls. The immunoblots are representative of 3 biological replicates.

(C) LNCaP cells were transfected with WT-EE-m*Plekhs1*-mEGFP, Y258F-EE-m*Plekhs1*-mEGFP, or vector alone, with or without constitutively active c-src. The cells were extracted and total PIP_3 quantified and normalized to total PI measured in the same sample. Data are mean ± SEM of 3 biological replicates. Statistics: two-way ANOVA with Holm-Šídák's multiple comparisons test.

(D and E) PIP arrays (D) and strips (E) were incubated with GFP-conjugated probes; PLEKHS1 WT (10–459), its isolated PH domain (10–134), or control protein (generated by the expression vector without a PLEKHS1 insert; 2x(10His)-MBP-mEGFP). The probes were visualized with anti-GFP primary and HRP-conjugated anti-mouse secondary antibodies. (D) The PIP arrays were spotted with a range of amounts (1.56–100 pmol) of eight synthetic phosphoinositides.

(F–G) Sucrose-loaded vesicles containing a mix of PS, PE, PC, sphingomyelin, and a range of concentrations of PIP_3 or PIP_2s (0.1–4 μM or 0.026–1 mol %) were incubated with GFP-conjugated iPH PLEKHS1. The assays were ultracentrifuged to sediment the liposomes, and aliquots pre- and post-sedimentation were resolved by SDS-PAGE and immunoblotted with an anti-GFP primary and HRP-conjugated anti-mouse secondary antibodies to determine the proportion of iPH that remained in the supernatant (G). Data were quantified (as a % of input remaining in the supernatant) from a minimum of 3 independent experiments (all the independent replicates are plotted) and are presented as mean ± SEM (F).

Please cite this article in press as: Chessa et al., PLEKHS1 drives PI3Ks and remodels pathway homeostasis in PTEN-null prostate, Molecular Cell (2023), https://doi.org/10.1016/j.molcel.2023.07.015

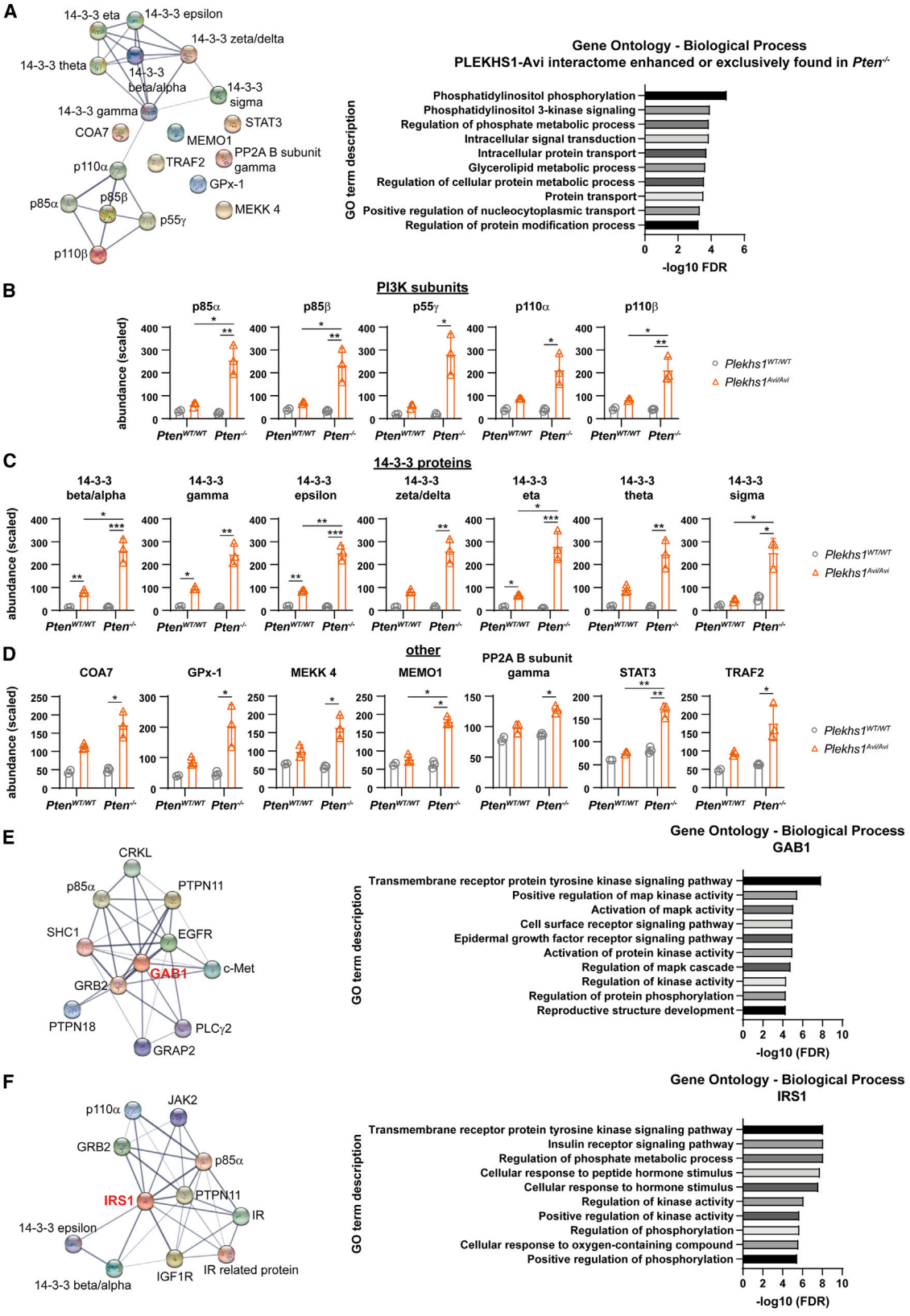

(legend on next page)

PI3K inhibitors is due to PI3K-driven activation of SFKs; rather, it is entirely explained by PIP_3/$PI(3,4)P_2$-driven, PH domain-mediated re-localization of PLEKHS1.

PIP_3 accumulation, AKT phosphorylation, and growth in PTEN-null but not WT prostate are dependent on PLEKHS1 in the prostate epithelium

To test whether PLEKHS1 was required for PIP_3 pathway activation in PTEN-KO mouse prostate, a *Plekhs1*$^{-/-}$ mouse model was derived using targeted embryonic stem cells (ESCs) (EUCOMM, *Plekhs1*$^{tm2a(EUCOMM)Hmgu}$). *Plekhs1*$^{-/-}$ mice were viable and without overt, prostate growth/morphology, or fecundity phenotypes (Figures S5A–S5D). The mice were interbred with *Pten*$^{loxP/loxP}$ and *PbCre4*$^{+}$ strains to obtain relevant genotypes for experiments (immunoblots confirmed PLEKHS1 and/or PTEN were lost from prostate organoids derived from these mice, as expected; see below, Figure S5E). Analysis of their prostates showed that PLEKHS1 was required for PIP_3 accumulation, AKT phosphorylation, tissue dysplasia, and growth in PTEN-KO but not WT tissue (Figures 6A–6E and S6D).

We addressed whether the PLEKHS1 dependency of PIP_3 accumulation and growth in PTEN-KO mouse prostate was prostate epithelium autonomous. Organoids derived from PTEN-KO prostate[41] grew more robustly and had substantially higher levels of PIP_3 and P-AKT and reduced levels of IRS1 compared to PTEN WT organoids (Figure S5F); the former three phenotypes were significantly dependent on PLEKHS1 expression (Figures 6F–6I and S5G), indicating that the phenotype of PLEKHS1-KO mouse prostate is a direct result of loss of PLEKHS1 function in prostate epithelial cells.

We also found IRS1 levels unaltered in PTEN-PLEKHS1-DKO (double knockout) prostate compared to PTEN-KO prostate (Figures S5H and S5I). Given that the loss of PLEKHS1 substantially rescues the PTEN-KO phenotype, this suggests that the reduction in IRS1 is not dependent on PLEKHS1 and alone is insufficient to drive these phenotypes.

We tested whether an SFK-PLEKHS1 axis was also important in mouse prostate organoids. We found that SFK-selective inhibitors reduced PIP_3 levels in PTEN-KO organoids substantially and relatively more than PTEN-PLEKHS1-DKO organoids (Figure 6H) and also reduced growth (as readout by organoid area) of both PTEN-KO and PTEN/PLEKHS1-DKO organoids (Figure 6I). These results suggest SFKs are relevant in this model and work largely upstream of PLEKHS1, consistent with them phosphorylating Y^{258}XXM-PLEKHS1.

Together, these results suggest that the high levels of PIP_3 and $PI(3,4)P_2$ in PTEN-KO prostate epithelial cells depend upon cell-intrinsic PLEKHS1. In the context of our conclusion, that PIP_3/$PI(3,4)P_2$ binding at the PH domain of PLEKHS1 is required for phosphorylation of Y^{258} and hence activation of class I PI3Ks, this suggests that a self-sustaining loop may have been established within PTEN-KO prostate epithelial cells.

There is also dramatic rewiring in other cancer models with activated PI3K signaling

We attempted to address the question "how widespread and consistent in detail is the dramatic network remodeling we have found in PTEN-KO mouse prostate?" by examining two further models of tumor progression.

Conditional expression of H1047R-p110α in mouse prostate epithelial cells (Figure S6A) causes hyperplasia by 100 days of age and invasive prostate carcinoma by 300 days, indicating that tumor progression driven by *Pik3ca* activation is slower than when driven by PTEN depletion (hyperplasia by 42 days of age and invasive carcinoma is prevalent by 200 days of age).[42] To assess potential network remodeling, we prepared lysates of flash-frozen 1-year-old H1047R-expressing, PTEN-KO, or WT dorso-lateral prostate lobes (note that in these samples *PBiCre* was used for both expression of H1047R-p110α and deletion of PTEN, a slightly different construct from the *PbCre4* promotor used in the main body of this work) and, as an additional control, dorso-lateral prostate lobes from 20-week-old mice that were either WT or PTEN-KO (*PbCre4*; i.e., identical to those used in Figure 1). Aliquots of the lysates were immunoblotted for P-AKT and P-$p70^{S6K}$ or immunoprecipitated with a p85α-directed antibody and subjected to label-free targeted proteomics to identify and semi-quantify associated IRS1 and PLEKHS1 (Figures S6B and S6C).

It was clear there was a relatively large amount of IRS1 and undetectable PLEKHS1 associated with p85α in the WT prostate, consistent with the data shown in Figure 1. We found significant but relatively small increases in P-T^{308}- and P-S^{473}-AKT (as reported previously[42]) and unchanged P-T^{389}-$p70^{S6K}$ in H1047R-p110α-expressing prostate lysates, implying relatively weak PI3K network activity compared to PTEN-KO prostate. In this context there was no significant increase in PLEKHS1, nor decrease in IRS1 (although there was a trend to reduction), association with p85α in the H1047R-p110α-positive prostate, while the PTEN-KO models showed changes in PLEKHS1 and IRS1 association similar to those in Figure 1.

Figure 4. Pulldown of endogenous PLEKHS1 shows that interactions with PI3Ks and 14:3:3 proteins are increased in PTEN-null tissue

(A) STRING network analysis (experimentally determined interactions) of specific PLEKHS1-Avi interactors (proteins recovered in significantly greater amounts in pulldowns from *Plekhs1*$^{Avi/Avi}$ × *mBirA*$^{+/-}$ compared to *Plekhs1*$^{WT/WT}$ × *mBirA*$^{+/-}$ tissue) that were recovered in significantly greater abundance from *Pten*$^{-/-}$ prostate, or exclusively found in *Pten*$^{-/-}$ prostate (12–15 weeks).

(B–D) Scaled abundances of PI3K subunits (B), 14-3-3 proteins (C), and other interactors (D) showing significant enrichment in *Plekhs1*$^{Avi/Avi}$ × *Pten*$^{WT/WT}$ and/or *Plekhs1*$^{Avi/Avi}$ × *Pten*$^{-/-}$ prostates (12–15 weeks) above their no-Avi controls (*Plekhs1*$^{WT/WT}$ × *Pten*$^{WT/WT}$ and/or *Plekhs1*$^{WT/WT}$ × *Pten*$^{-/-}$) as calculated in Proteome Discoverer software. The experiment was run as a single cohort of n = 3 biological replicates per genotype, except *Plekhs1*$^{WT/WT}$ × *Pten*$^{-/-}$, where n = 2. Statistics: two-way ANOVA with adjusted p values calculated using the Benjamini-Hochberg method. Adjusted p value summaries <0.05 are indicated. Data are mean ± SEM or mean ± range (n = 2).

(E and F) STRING network analysis (experimentally determined interactions) of mouse GAB1 (E) and mouse IRS1 (F). A maximum number of 10 interactions is shown.

(A, E, and F) Network nodes represent proteins; edges represent protein-protein associations, including functional and physical interactions. Line thickness indicates the strength of data support. See also Figures S3 and S4.

Please cite this article in press as: Chessa et al., PLEKHS1 drives PI3Ks and remodels pathway homeostasis in PTEN-null prostate, Molecular Cell (2023), https://doi.org/10.1016/j.molcel.2023.07.015

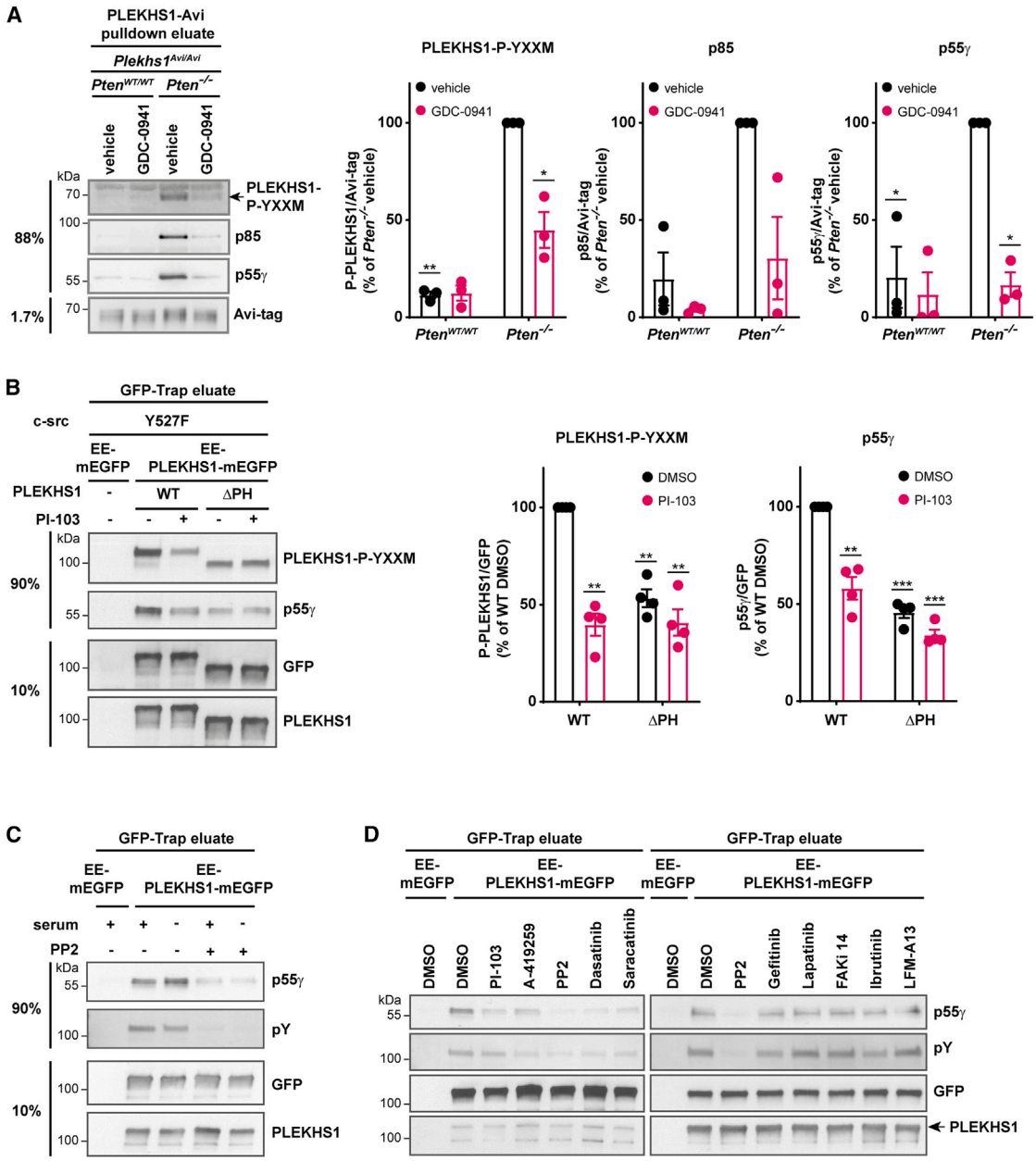

Figure 5. Y^{258}XXM-PLEKHS1 is phosphorylated in a PI3K- and Src-family kinase-dependent fashion

(A) PLEKHS1-Avi was pulled down from prostate lysates from $Pten^{WT/WT}$ or $Pten^{-/-}$ mice (all expressing $mBirA^{+/-}$, 12–15 weeks) that had been treated with either vehicle or PI3Ki (GDC-0941, 800 mg/kg/day for 2 days). Phosphorylation of PLEKHS1 on Y^{258}XXM and recovery of total p85 and p55γ were quantified by immunoblotting as indicated. Data were obtained from 3 independent experiments (in each experiment a minimum of 3 prostates were pooled from $Pten^{WT/WT}$ mice and a minimum of 2 prostates were pooled from $Pten^{-/-}$ mice) and are presented in the form of percentages of the vehicle-treated, $Plekhs1^{Avi/Avi}$ × $Pten^{-/-}$ samples and are mean ± SEM. Statistics: multiple two-tailed, one-sample t tests on baseline-corrected data (all compared to the data defining 100%), with Holm-Šídák's correction. Adjusted p value summaries <0.05 are indicated.

(B) GFP-trap pulldown from LNCaP cells following co-transfection with tagged wild-type (WT) or Δ PH mPLEKHS1 (EE-WT- or Δ PH-PLEKHS1-mEGFP) and activated (Y527F)-c-src. Empty vector (EE-mEGFP) was included as a negative control. Cells were pretreated with either vehicle (0.1% DMSO) or PI3K inhibitor (PI-103, 2 μM) for 1 h. Lysates were subjected to GFP-trap pulldown and eluates were immunoblotted with the indicated antibodies to measure PLEKHS1-P-YXXM and recovery of p55γ, with GFP and PLEKHS1 immunoblots as loading controls (left panel, representative image). Data were obtained from 4 independent experiments (right panel) and are mean ± SEM. Statistics: multiple two-tailed, one-sample t tests (comparisons to WT DMSO). Adjusted p value summaries <0.05 are indicated.

(C) GFP-trap pulldown from LNCaP cells following co-transfection with tagged wild-type (WT) mPLEKHS1 (EE-WT-PLEKHS1-mEGFP). Empty vector (EE-mEGFP) was included as a negative control. Cells were serum starved (16 h) and pre-treated with either vehicle DMSO (0.1%) or SFK-inhibitor PP2 (10 μM). Eluates were immunoblotted to assay PLEKHS1 interaction with p55γ and PLEKHS1 total Tyr phosphorylation (n = 2).

(legend continued on next page)

Please cite this article in press as: Chessa et al., PLEKHS1 drives PI3Ks and remodels pathway homeostasis in PTEN-null prostate, Molecular Cell (2023), https://doi.org/10.1016/j.molcel.2023.07.015

SHIP2 and PTEN were conditionally deleted in the ovary (Figure S6D), and this led to the emergence of a rapidly growing sex cord-gonadal stromal tumor (distinct to the epithelial tumors in PTEN-KO prostrate) (Figure S6D). We performed experiments similar to those described for H1047R-p110α-positive prostate on WT or 3-, 4-, and 6-month-old SHIP2/PTEN-DKO ovaries with 12-week-old WT or PTEN-KO prostate as a control.

In WT ovary, it was clear that the major PI3K interactor, of those we targeted, was IRS1 (Figure S6E), consistent with the idea that in healthy ovary, like prostate, the dominant physiological driver of the PI3K network is the insulin/IGF/IRS pathway. Further, and also consistent with our findings in the prostate tumor model, both the levels of IRS1 (Figure S6F) and its association with p85α (Figure S6E) were dramatically reduced in DKO ovaries.

We found large increases in phosphorylation of AKT and of SFKs but surprisingly little evidence of increased P-T^{389}-p70^{S6K} in lysates from 3-, 4-, and 6-month-old DKO ovary (though the P-T^{389}-p70^{S6K} signal was high in WT ovary compared to WT prostate) (Figure S6F). It was clear that lysates of WT or DKO mouse ovary expressed far less PLEKHS1 than prostate (Figure S6F), in line with our finding that PLEKHS1 has a very restricted tissue distribution in the mouse (Figures S3E and S3F) and the reported distribution of PLEKHS1 mRNA. However, the levels of PLEKHS1 increased significantly in lysates from 4-month-old to 6-month-old DKO ovary compared to WT (Figure S6F). Further, there was a significant increase in association of PLEKHS1 with p85α in 4-month-old DKO ovary compared to WT, but this was substantially lower than the levels of PLEKHS1 associated with p85α in PTEN-KO prostate (Figure S6E). Interestingly, association of AFAP1L2 with p85α was dramatically increased in DKO ovary compared to WT and PTEN-KO prostate (Figure S6E). BCAP association with p85α was also increased in DKO ovary, to relative levels similar to those seen in PTEN-KO prostate (Figure S6E).

These results suggest, unsurprisingly, that there is intense PI3K network activation and pathway feedback in DKO ovary, with the outcome that levels and binding of IRS1 to p85α are dramatically reduced. There is further pathway remodeling, including a small increase in PLEKHS1 association with PI3Ks along with relatively far greater increases in AFAP1L2 and BCAP (in prostate we argued the BCAP was probably located in infiltrating immune cells because of correlated changes in p110δ and CSF1R and their known distributions, but in the absence of these additional correlates, it is less clear this is the case in the DKO ovary). This suggests that PLEKHS1 may have a role in the phenotype of DKO ovary but potentially less significant than that of AFAP1L2 and possibly BCAP.

Collectively, these results indicate PLEKHS1 does not have a ubiquitous role in remodeling in constitutively activated PI3K networks. It may have roles that are a function of its expression levels and the intensity of PI3K pathway activation and feedback, but other PI3K activators/adaptors may take on more important roles in other tissues. However, the striking drop in IRS drive into the PI3K network in settings with oncogenic constitutive PI3K pathway activation is probably a more universal and key event in the tumor progression process.

PI3K pathway rewiring is relevant in human prostate cancer

Previous studies have reported that PI3K/AKT/mTOR pathway activation can occur without proteogenomic associations with putative drivers or mutations in a large subset of prostate cancers.[43,44] Although *PTEN* deletion occurs commonly (~17%) in primary prostate cancers, it correlates poorly with pathway activation in cohort analysis, likely due to confounding effects of alternate mechanisms of PI3K pathway deregulation (e.g., *SPOP* mutation).[10,43] Lack of predictive biomarkers for pathway activation presents a major challenge for therapeutic PI3K targeting and patient stratification. OncoPrint analysis of TCGA prostate adenocarcinoma (TGGA-PRAD) datasets confirmed that *PTEN* alterations occur commonly in primary prostate cancers (26%), the vast majority of which are genetic deletion or inactivation and/or mRNA downregulation (Figure 7A). Although *IRS1* and *PLEKHS1* mutations were rare (0.6% and 1%, respectively), *IRS1* expression was frequently downregulated, whereas a substantial number of cases showed *PLEKHS1* upregulation (Figure 7A). In the context that h*PLEKHS1* is expressed in both healthy and cancerous prostate, we investigated TCGA-PRAD datasets for evidence of PI3K pathway rewiring. *IRS1* gene expression was significantly decreased (Figure 7B), and *PLEKHS1* gene expression was significantly increased in primary and metastatic prostate tumors compared to healthy tissue (Figures 7C and S7A). In sample subsets harboring low *PTEN* expression, *IRS1* gene expression was significantly lower and *PLEKHS1* expression significantly higher compared to sample subsets with normal *PTEN* expression (Figures 7D and 7E). Changes in *PLEKHS1* mRNA expression were queried further as they correlated with protein levels in cancer types where proteomics data were available, and furthermore, we have shown that simple over-expression of WT but not Y^{258}F-mutant PLEKHS1 in LNCaP cells can increase PIP_3 (Figure 3C). Grouped comparison of primary prostate cancers based on quartiles of *PLEKHS1* mRNA expression (Figure S7B) showed significant positive correlations with activation of key pathway proteins (AKT, 4E-BP1, and S6 phosphorylation) (Figures 7F, S7D, and S7E). Furthermore, Src-Y419^{419} phosphorylation also correlated strongly with PI3K pathway activation in primary prostate cancers, in agreement with previous reports[43] (Figures 7G and S7C). Collectively, these findings suggest that PI3K pathway rewiring takes place in the context of PI3K pathway hyperactivation in human prostate cancer.

A similar analysis of TCGA-BRCA and TCGA-UCEC datasets revealed that *PLEKHS1* expression, as well as Src-Y^{419} phosphorylation, showed significant positive correlations with AKT phosphorylation in both cancer types (Figures S7F, S7G, S7I,

(D) Cells were pre-treated with vehicle (0.1% DMSO); PI3K inhibitor (2 μM PI-103); Src-family kinase inhibitors A-419259 (1 μM), PP2 (10 μM), Dasatinib (100 nM), or Saracatinib (1 μM); EGFR inhibitor Gefitinib (10 μM); EGFR/Her2 inhibitor Lapatinib (10 μM); FAK inhibitor FAKi 14 (10 μM); BTK inhibitor Ibrutinib (1 μM); or Tec-family kinase inhibitor LFM-A13 (20 μM) for 1 h. Eluates were immunoblotted with anti-p55γ and anti-phosphotyrosine (total) antibodies to assay endogenous phosphorylation of Y^{258}XXM-PLEKHS1, with GFP and PLEKHS1 as input controls (n = 2, except results with PP2, which are n = 3). See also Figure S4.

Please cite this article in press as: Chessa et al., PLEKHS1 drives PI3Ks and remodels pathway homeostasis in PTEN-null prostate, Molecular Cell (2023), https://doi.org/10.1016/j.molcel.2023.07.015

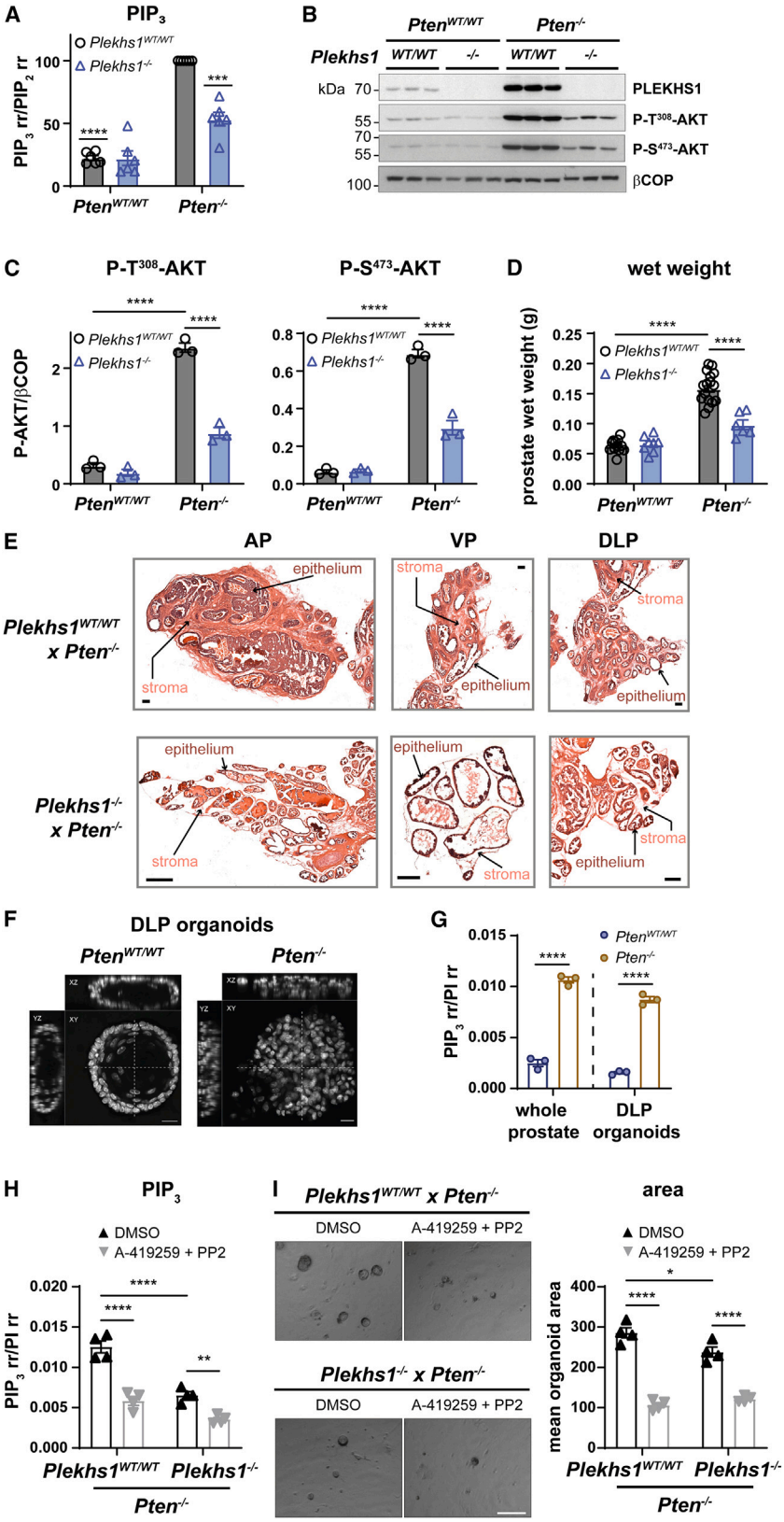

Figure 6. PIP_3 accumulation, AKT phosphorylation, and growth in PTEN-null but not wild-type prostate are dependent on PLEKHS1 in the prostate epithelium

Whole prostates were rapidly dissected from mice (12–15 weeks) with indicated genotypes.

(A) Flash frozen material was extracted, and total PIP_3 was quantified, normalized to total PIP_2 quantified in the same sample, and presented as a % of the amount found in *Plekhs1*$^{WT/WT}$ × *Pten*$^{-/-}$ samples. Data are mean ± SEM of 6 biological replicates per genotype. Statistics: multiple two-tailed, one-sample t tests, with Holm-Šídák's correction. Significant p value summaries ($p \leq 0.05$) are indicated.

(B and C) Frozen prostate was solubilized and immunoblotted with the indicated antibodies. P-T^{308}- and P-S^{473}-AKT were quantified relative to the amount of βCOP in the same samples by immunoblotting. (C) Data are mean ± SEM of n = 3 biological replicates per genotype.

(D) Prostate wet weights from mice of the indicated genotypes. Data are mean ± SEM (n = 12, *Plekhs1*$^{WT/WT}$ × *Pten*$^{WT/WT}$; n = 8, *Plekhs1*$^{-/-}$ × *Pten*$^{WT/WT}$; n = 24, *Plekhs1*$^{WT/WT}$ × *Pten*$^{-/-}$; and n = 6, *Plekhs1*$^{-/-}$ × *Pten*$^{-/-}$ biological replicates).

(E) H&E-stained cryosections of prostates taken from the indicated lobes and genotypes. AP, anterior prostate; VP, ventral prostate; DLP, dorsolateral prostate. Representative images from n = 3 biological replicates are shown. Scale bars: 200 μm.

(F–I) DLP lobes from *Pten*$^{WT/WT}$ and *Pten*$^{-/-}$ mouse prostates (12–15 weeks) were used to derive organoids.

(F) DLP organoids were fixed, stained with DAPI to reveal nuclei, and visualized by confocal microscopy. The images were constructed from z stacks of confocal sections and show a mid-level section through the organoids. Scale bars: 20 μm.

(G) PIP_3 measurements in whole prostate tissue and DLP organoids. Data are mean ± SEM of 3 biological replicates per genotype and are expressed as the ratio of the abundance of total PIP_3 to that of total PI in the same sample.

(H) PIP_3 measurements in *Plekhs1*$^{WT/WT}$ × *Pten*$^{-/-}$ and *Plekhs1*$^{-/-}$ × *Pten*$^{-/-}$ DLP organoids treated with either vehicle (DMSO; 0.11%) or SFK inhibitors A-419259 (1 μM) + PP2 (10 μM). Data are mean ± SEM of 4 biological replicates per genotype and are expressed as the ratio of the abundance of total PIP_3 to that of total PI in the same sample.

(I) Transmitted light images from *Plekhs1*$^{WT/WT}$ × *Pten*$^{-/-}$ and *Plekhs1*$^{-/-}$ × *Pten*$^{-/-}$ DLP organoids, cultured in the presence of vehicle (DMSO; 0.11%) or SFK inhibitors A-419259 (1 μM) + PP2 (10 μM). A representative image is shown for each genotype. Data are mean ± SEM (n = 4 biological replicates per genotype where each data point is an average area of 10–82 organoids).

Statistics of (C), (D), (G), (H), and (I): two-way ANOVA with Holm-Šídák's multiple comparisons tests. Significant p value summaries ($p \leq 0.05$) are indicated. See also Figure S5.

Please cite this article in press as: Chessa et al., PLEKHS1 drives PI3Ks and remodels pathway homeostasis in PTEN-null prostate, Molecular Cell (2023), https://doi.org/10.1016/j.molcel.2023.07.015

CellPress
OPEN ACCESS

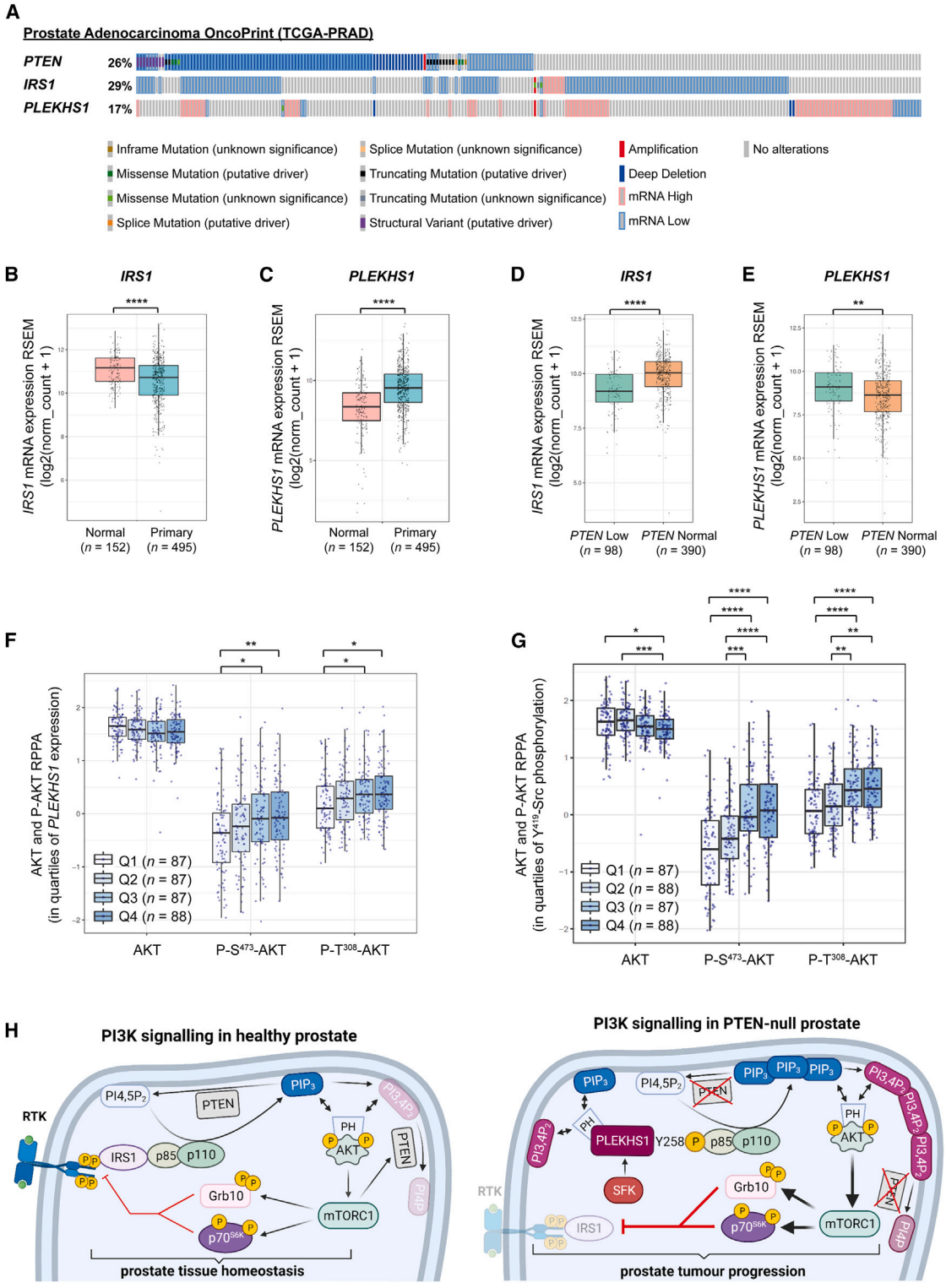

Figure 7. PI3K pathway rewiring is relevant in human prostate cancer

(A) OncoPrint data represent genetic alterations and mRNA expression data of *PTEN*, *IRS1*, and *PLEKHS1* in patient-matched samples from TCGA PanCancer atlas (TCGA-PRAD), cBioPortal.[45,46] Types of genetic alteration (indicated below) include mRNA upregulation ("mRNA high") and mRNA downregulation ("mRNA low") relative to normal samples (log RNA Seq V2 RSEM; *Z* score threshold ±2.0).

(legend continued on next page)

Please cite this article in press as: Chessa et al., PLEKHS1 drives PI3Ks and remodels pathway homeostasis in PTEN-null prostate, Molecular Cell (2023), https://doi.org/10.1016/j.molcel.2023.07.015

and S7J). *PIK3CA* mutations are the most prevalent genetic alteration in the PI3K pathway in breast cancer.[48] Interestingly, *PLEKHS1* expression was significantly increased in *PIK3CA*-mutated compared to *PIK3CA*-WT samples in breast invasive carcinoma but unaltered in PTEN-mutated samples (Figure S7H). Genetic alterations in *PTEN*, *PIK3CA*, and *PIK3R1* are common in endometrial cancers, with alterations in PTEN being the most common.[49–51] *PLEKHS1* expression was significantly elevated in *PTEN*-mutated compared to *PTEN*-WT uterine endometroid carcinoma and unaltered in *PIK3CA*-mutated and *PIK3R1*-mutated cancers (Figure S7K).

Overall, these findings support the broader clinical relevance of a Src-PLEKHS1-PI3K signaling axis in human cancers.

DISCUSSION

Our data and past work show that there is a large increase in SFK expression and activity in PTEN-KO mouse prostate, and this is thought to be an important driver of remodeling of the phosphotyrosine landscape and disease progression.[52,53] Our results suggest part of the impact of SFKs may be via phosphorylation of PLEKHS1.

A number of lines of evidence suggest that in the absence of PTEN the PI3K pathway could become relatively insensitive to the receptor mechanisms that are key regulators of its activity in healthy prostate: (1) the dramatic reductions in binding of p85s to IRS, EGFR, and SHC1 (a receptor-proximal adaptor) in PTEN-KO prostate; (2) the potential for PLEKHS1 to be subject to positive feedback from PI3Ks; (3) the lack of RTKs and their adaptors in the STRING network of PLEKHS1 compared to GAB and IRS proteins; (4) the insensitivity of YXXM phosphorylation of PLEKHS1 in LNCaP cells to serum starvation; (5) work demonstrating that tumors with activating mutations in the PI3K pathway, including mouse prostate-specific loss of PTEN, are insensitive to dietary restriction[54]; and, finally, (6) the possibility that SFKs could be activated by ROS in PTEN-KO prostate.

We propose a qualitative model (Figure 7H) that can rationalize our results. In healthy prostate the PI3K pathway is driven by extracellular ligands controlling tyrosine phosphorylation of IRSs. It is constrained by a combination of $PI(3,4)P_2/PIP_3$ phosphatases, particularly PTEN, and pathway feedback. These counter-poised factors establish a homeostatic mechanism that shapes the output of the pathway and governs tissue growth. Upon loss of PTEN activity, the levels of $PIP_3/PI(3,4)P_2$ and pathway activity are increased, but limited by feedback, reducing IRS inputs. The increase in $PI(3,4)P_2/PIP_3$ is well matched to the selectivity of the PH domain of PLEKHS1 and causes its localization to membranes. SFKs are more active in PTEN-KO cells, in part as a result of ROS-induced sulfenylation and part via the loss of protein phosphatase activity of PTEN leading to de-repression of PTK6 and Src.[13,15] This leads to increased phosphorylation of PLEKHS1 on Y^{258} and a further increase in PI3K activity. As a result, and in the context of the suppression of IRS signaling and the insensitivity of PLEKHS1 to feedback, PLEKHS1 becomes a major activator of the PI3K pathway. In this setting the PI3K pathway might become less dependent on growth factor drive to maintain its activity.

Our results suggest that PLEKHS1 signaling may be limited by association with 14:3:3 proteins. Three phosphoserine residues in PLEKHS1 are predicted to bind 14:3:3 proteins[55] (ranked predicted sites: S^{157}, S^{256}, and S^{180}), all of which are more heavily phosphorylated in PTEN-KO prostate (Figure S4A). S^{256} is also very close to the Y^{258} site that can bind to p85 and may therefore establish a competition between p85 and 14:3:3 binding, similar to the role of 14:3:3 proteins in the termination of signaling by GAB2.[56] This suggests that PLEKHS1 is either complexed to 14:3:3 proteins or PI3Ks, and that conclusion is supported by STRING analysis of the family of specific PLEKHS1 interactors we have defined (Figure 4A).

Another protein that was substantially more abundant in p85 pulldowns from PTEN-KO mouse prostate is AFAP1L2 (XB130). It harbors a Y^{54}XXM motif, demonstrated to bind and activate PI3K signaling.[57] The two PH domains in AFAP1L2 are unlikely to bind phosphoinositides, but AFAP1L2 interacts with SH3PXD2A/TKS5/FISH,[58] a PX-domain-containing adaptor that can bind $PI(3,4)P_2$[59] and can be phosphorylated by Src.[60] Numerous studies suggest that AFAP1L2 can drive tumor progression.[61] Our observations suggest that AFAP1L2 may contribute to pathway remodeling and tumor progression in both the PTEN-KO prostate and PTEN/SHIP2-DKO ovary mouse models and perhaps more importantly in the latter.

PLEKHS1 appears to be more widely expressed in human tissues than mouse, so cancers in more cell/tissue types might gain advantage from the ability of PLEKHS1 to sustain chronic activation of the PIP_3 network. This idea is supported by work that has positively linked PLEKHS1 to tumor progression in a range of tissues, including gastric, colorectal, hepatocellular, and thyroid as

(B and C) *IRS1* mRNA expression (RSEM) (B) and *PLEKHS1* mRNA expression (RSEM) (C) in normal prostate and primary prostate cancer. Data are from UCSC Xena database (TCGA PanCancer, TCGA Target, GTEx[47]). Statistics: Welch's t test.

(D and E) *IRS1* mRNA expression (RSEM) (D) and *PLEKHS1* mRNA expression (RSEM) (E) in *PTEN* Low and *PTEN* Normal samples. *PTEN* Low samples represent those with a Z score of ≤ -2.0 in the tumor sample, relative to normal sample. *PTEN* Normal samples represent those with a Z score > -2.0 in the tumor sample, relative to normal sample. Data are from cBioPortal TCGA-PRAD. Statistics: Welch's t test.

(F) Primary prostate cancer samples were grouped by quartiles of *PLEKHS1* mRNA expression (RSEM) and compared for AKT, P-S^{473}-AKT, and P-T^{308}-AKT protein levels (RPPA). Data are from cBioPortal TCGA-PRAD. Statistics: Kruskal-Wallis with Dunn's multiple comparison test.

(G) Primary prostate cancer samples were grouped by quartiles of P-Y^{419}-Src protein levels (RPPA) and compared for AKT, P-S^{473}-AKT, and P-T^{308}-AKT protein levels (RPPA). Data are from cBioPortal TCGA-PRAD. Statistics: Kruskal-Wallis with Dunn's multiple comparison test.

(H) Model for PI3K signaling in healthy and PTEN-null prostate. In healthy prostate, PI3K signaling is mainly driven by IRS family members and fine-tuned by PTEN activity and two forms of feedback from mTORC1: firstly, via $p70^{S6K}$ and Grb10, reduced expression of RTKs and IRS leading to reduced activation of PI3Ks, and secondly, via 4E-BP1, increased synthesis and accumulation of PTEN. In *Pten*$^{-/-}$ prostate, the PI3K signaling network is dramatically re-wired. PLEKHS1 becomes a major activator and target of PI3K signaling, sustaining pathway activity despite intense negative feedback. We propose that re-wiring of PI3K signaling underpins *Pten*$^{-/-}$ prostate tumor progression. See also Figure S7.

well as prostate cancers[62–68] (one study reported a negative correlation[69]). Consistent with the majority of those studies, heterologous over-expression of hPLEKHS1 has been reported to increase AKT phosphorylation and invasiveness in thyroid cancer cells.[66] This is clearly supported by our bioinformatic work correlating *PLEKHS1* mRNA with P-AKT levels and *PTEN* or *PIK3CA* mutational status in uterine endometrioid cancer or breast invasive carcinoma (Figures S7F–S7K).

Several studies have also reported a hot-spot of somatic, non-coding mutations at the apex of a palindromic hairpin in the first intron of PLEKHS1 in cancer. These mutations are at their most frequent in bladder cancer, where they occur in 40% of cases.[70] Further work suggests they result from high APOBEC activity in the cancer.[71–74] They correlate with reduced *PLEKHS1* expression in some studies,[70,74] but others find no correlation.[75] It remains unclear whether these non-coding mutations produce an impact via PLEKHS1 expression.

Our results with multiple mouse models suggest that PI3K pathway remodeling is a universal feature of cancers driven by hyperactivated PI3K signaling. Indeed, the substantial loss of IRS proteins in PTEN-KO mouse prostate and PTEN/SHIP2-DKO mouse ovary as a result of PI3K pathway feedback appears to be a pivotal event in tumor progression. Not only does it play a key role in shifting the tumor toward a freedom from the requirement for growth factor/diet-based permission to enter an anabolic/growth state, it appears to allow adaptors that are not subject to pathway feedback such as PLEKHS1 (and probably AFAP1L2) to become more influential. The outcome is that a more cell-autonomous, higher set-point for pathway activity is established, thus priming the cell to take advantage of further oncogenic mutations. This points to the potential for identifying new vulnerabilities in the PI3K network in cancer cells.

Limitations of the study

Our data suggest SFKs may be responsible for phosphorylating the key Y^{258}XXM motif in PLEKHS1; however, we have not identified the specific members that are required *in vivo*, and this will be important to define the best strategy to inhibit PLEKHS1 function. Both pathway remodeling and the *in vivo* functions of PLEKHS1 are poorly replicated in cell lines, and although mouse organoids have provided insights, they are challenging to work with. This has limited the mechanistic studies, such as visualizing the distribution of PLEKHS1 or knocking-in point-mutant versions of IRS proteins, which have been plausible.

STAR★METHODS

Detailed methods are provided in the online version of this paper and include the following:

- KEY RESOURCES TABLE
- RESOURCE AVAILABILITY
  - Lead contact
  - Materials availability
  - Data and code availability
- EXPERIMENTAL MODEL AND STUDY PARTICIPANT DETAILS
  - Experimental animals
  - Experimental procedures
  - Ethical statement
  - Housing and husbandry
  - Animal care and monitoring
  - Study design, sample size and Randomisation
  - Cell lines
- METHOD DETAILS
  - Prostate isolation and streptavidin-mediated pulldown of avi-tagged proteins
  - Immunoprecipitation
  - TMT-LC-MS/MS
  - $p85^{Avi/avi}$ interactome analysis
  - *Plekhs1*$^{Avi/avi}$ interactome analysis
  - Label-free, targeted LC-MS protein analyses
  - GFP-trap pulldown assay
  - Generation of custom-made antibodies
  - Western blot
  - Imaging
  - Measurement of PIP_3
  - Cloning of Plekhs1 from mouse prostate and generation of bacterial and mammalian expression constructs
  - Recombinant protein expression and purification
  - Lipid binding assays
  - Flow cytometry
  - Bioinformatics analysis
- QUANTIFICATION AND STATISTICAL ANALYSIS
  - General statistical analyses

SUPPLEMENTAL INFORMATION

Supplemental information can be found online at https://doi.org/10.1016/j.molcel.2023.07.015.

ACKNOWLEDGMENTS

The work was supported by grants from the BBSRC (BB/P013384/1 and BB/P020240/1), the MRC (MR/R000409/1), an ITN PhD studentship (to P.J.), a CRUK Cambridge Center PhD (to A.A.), and a TAG grant from the KEC program at the Babraham Institute (BI). We would like to thank Professor Vincent Gnanapragasam (Translational Prostate Cancer Group, CRUK Cambridge Cancer Center, UK), Clive D'Santos (Proteomics, CRUK, Cambridge Institute), and Antonio Ramos-Montoya and Ajoeb Baridi (CRUK, Cambridge Institute, at that time) for helpful discussions; Estere Seinkmane for culturing organoids; the staff in BSU at BI for mouse work; Judith Webster for sample preparation for mass spectrometry analysis; Keith Davidson (BI, Signaling) for technical assistance; Attila Bebes, Aleksandra Lazowska-Addy, and Rachael Walker (BI, Flow Facility) for help with cell sorting experiments; Elena Ivanova (BI, Epigenetics) for help with cryo-sectioning and ovary dissections; Felix Krueger (BI, Bioinformatics, at that time) for help analyzing mRNA-seq data; and Chiranjeevi Sandi (AZ, Cambridge, at that time) for sharing unpublished mRNA-seq data.

AUTHOR CONTRIBUTIONS

T.A.M.C. contributed to conception of the project, performed and analyzed experiments, prepared figures, and wrote the manuscript; P.J. created GM-PLEKHS1 strains, performed experiments, and analyzed their data; A.A. performed experiments, analyzed data, and prepared figures and text for the manuscript; S.S. performed experiments, analyzed data, and prepared figures and text for the manuscript; K.E.A. performed lipid analysis; D.B. optimized FACS-sort experiments with cells from mouse prostate; A.K. performed lipid analysis; B.A.S. prepared an anti-Avi monoclonal antibody and prepared organoids; I.W.L. helped perform experiments with cell lines; S.F. analyzed histochemical

slides; D.J.T. generated samples from *PBiCre*$^{+/-}$ *Pik3ca*$^{+/Lat\text{-}H1047R}$ mice; W.A.P. generated the *PBiCre*$^{+/-}$ *Pik3ca*$^{+/Lat\text{-}/H1047R}$ transgenic line; H.B.P. managed the *PBiCre*$^{+/-}$ *Pik3ca*$^{+/Lat\text{-}H1047R}$ mouse sample preparation and contributed to interpretation of results; J.S. generated PTEN/SHIP2-DKO mice and prepared samples for analysis; T.S. generated PTEN/SHIP2-DKO mice, shared associated data, and contributed to the interpretation of our results; D.O. performed proteomic workflow and data analysis; D.S. performed generation of GM mouse models; A.S.-P. provided statistical expertise and generated the heatmap; M.W. provided structural insight into PLEKHS1 protein and domain expression; S.W. performed confocal analysis of organoids; H.O. created image analysis pipelines; S.C. contributed to grant writing, planning, and writing of the manuscript; P.T.H. and L.R.S. conceived the project, wrote grants, planned experiments, interpreted data, and wrote the manuscript.

DECLARATION OF INTERESTS

S.C. is an employee of AZ. We, the authors, have a patent related to this work (patent application number 2304156.9, granted by United Kingdom Patent Office, covering "modulating PLEKHS1 activity in a cell").

INCLUSION AND DIVERSITY

We support inclusive, diverse and equitable conduct of research.

Received: September 22, 2022
Revised: May 5, 2023
Accepted: July 13, 2023
Published: August 10, 2023

REFERENCES

1. Fruman, D.A., Chiu, H., Hopkins, B.D., Bagrodia, S., Cantley, L.C., and Abraham, R.T. (2017). The PI3K Pathway in Human Disease. Cell *170*, 605–635. https://doi.org/10.1016/j.cell.2017.07.029.
2. Leslie, N.R., Biondi, R.M., and Alessi, D.R. (2001). Phosphoinositide-regulated kinases and phosphoinositide phosphatases. Chem. Rev. *101*, 2365–2380. https://doi.org/10.1021/cr000091i.
3. Maehama, T., and Dixon, J.E. (1998). The tumor suppressor, PTEN/MMAC1, dephosphorylates the lipid second messenger, phosphatidylinositol 3,4,5-trisphosphate. J. Biol. Chem. *273*, 13375–13378. https://doi.org/10.1074/jbc.273.22.13375.
4. Malek, M., Kielkowska, A., Chessa, T., Anderson, K.E., Barneda, D., Pir, P., Nakanishi, H., Eguchi, S., Koizumi, A., Sasaki, J., et al. (2017). PTEN Regulates PI(3,4)P(2) Signaling Downstream of Class I PI3K. Mol. Cell *68*, 566–580.e10. https://doi.org/10.1016/j.molcel.2017.09.024.
5. Li, J., Yen, C., Liaw, D., Podsypanina, K., Bose, S., Wang, S.I., Puc, J., Miliaresis, C., Rodgers, L., McCombie, R., et al. (1997). PTEN, a putative protein tyrosine phosphatase gene mutated in human brain, breast, and prostate cancer. Science *275*, 1943–1947. https://doi.org/10.1126/science.275.5308.1943.
6. Liu, W., James, C.D., Frederick, L., Alderete, B.E., and Jenkins, R.B. (1997). PTEN/MMAC1 mutations and EGFR amplification in glioblastomas. Cancer Res. *57*, 5254–5257.
7. Steck, P.A., Pershouse, M.A., Jasser, S.A., Yung, W.K., Lin, H., Ligon, A.H., Langford, L.A., Baumgard, M.L., Hattier, T., Davis, T., et al. (1997). Identification of a candidate tumour suppressor gene, MMAC1, at chromosome 10q23.3 that is mutated in multiple advanced cancers. Nat. Genet. *15*, 356–362. https://doi.org/10.1038/ng0497-356.
8. Teng, D.H., Hu, R., Lin, H., Davis, T., Iliev, D., Frye, C., Swedlund, B., Hansen, K.L., Vinson, V.L., Gumpper, K.L., et al. (1997). MMAC1/PTEN mutations in primary tumor specimens and tumor cell lines. Cancer Res. *57*, 5221–5225.
9. Samuels, Y., Wang, Z., Bardelli, A., Silliman, N., Ptak, J., Szabo, S., Yan, H., Gazdar, A., Powell, S.M., Riggins, G.J., et al. (2004). High frequency of mutations of the PIK3CA gene in human cancers. Science *304*, 554. https://doi.org/10.1126/science.1096502.
10. Blattner, M., Liu, D., Robinson, B.D., Huang, D., Poliakov, A., Gao, D., Nataraj, S., Deonarine, L.D., Augello, M.A., Sailer, V., et al. (2017). SPOP Mutation Drives Prostate Tumorigenesis In Vivo through Coordinate Regulation of PI3K/mTOR and AR Signaling. Cancer Cell *31*, 436–451. https://doi.org/10.1016/j.ccell.2017.02.004.
11. Vanhaesebroeck, B., Perry, M.W.D., Brown, J.R., André, F., and Okkenhaug, K. (2021). PI3K inhibitors are finally coming of age. Nat. Rev. Drug Discov. *20*, 741–769. https://doi.org/10.1038/s41573-021-00209-1.
12. Burke, J.E. (2018). Structural Basis for Regulation of Phosphoinositide Kinases and Their Involvement in Human Disease. Mol. Cell *71*, 653–673. https://doi.org/10.1016/j.molcel.2018.08.005.
13. Alwanian, W.M., Vlajic, K., Bie, W., Kajdacsy-Balla, A., and Tyner, A.L. (2022). Protein tyrosine kinase 6 regulates activation of SRC kinase. J. Biol. Chem. *298*, 102584. https://doi.org/10.1016/j.jbc.2022.102584.
14. Heppner, D.E., Dustin, C.M., Liao, C., Hristova, M., Veith, C., Little, A.C., Ahlers, B.A., White, S.L., Deng, B., Lam, Y.W., et al. (2018). Direct cysteine sulfenylation drives activation of the Src kinase. Nat. Commun. *9*, 4522. https://doi.org/10.1038/s41467-018-06790-1.
15. Wozniak, D.J., Kajdacsy-Balla, A., Macias, V., Ball-Kell, S., Zenner, M.L., Bie, W., and Tyner, A.L. (2017). PTEN is a protein phosphatase that targets active PTK6 and inhibits PTK6 oncogenic signaling in prostate cancer. Nat. Commun. *8*, 1508. https://doi.org/10.1038/s41467-017-01574-5.
16. Shah, N.H., Löbel, M., Weiss, A., and Kuriyan, J. (2018). Fine-tuning of substrate preferences of the Src-family kinase Lck revealed through a high-throughput specificity screen. Elife *7*, e35190. https://doi.org/10.7554/eLife.35190.
17. Songyang, Z., Carraway, K.L., 3rd, Eck, M.J., Harrison, S.C., Feldman, R.A., Mohammadi, M., Schlessinger, J., Hubbard, S.R., Smith, D.P., Eng, C., et al. (1995). Catalytic specificity of protein-tyrosine kinases is critical for selective signalling. Nature *373*, 536–539. https://doi.org/10.1038/373536a0.
18. Miller, W.T. (2003). Determinants of substrate recognition in nonreceptor tyrosine kinases. Acc. Chem. Res. *36*, 393–400. https://doi.org/10.1021/ar020116v.
19. Shvartsman, D.E., Donaldson, J.C., Diaz, B., Gutman, O., Martin, G.S., and Henis, Y.I. (2007). Src kinase activity and SH2 domain regulate the dynamics of Src association with lipid and protein targets. J. Cell Biol. *178*, 675–686. https://doi.org/10.1083/jcb.200701133.
20. Moon, K.D., Post, C.B., Durden, D.L., Zhou, Q., De, P., Harrison, M.L., and Geahlen, R.L. (2005). Molecular basis for a direct interaction between the Syk protein-tyrosine kinase and phosphoinositide 3-kinase. J. Biol. Chem. *280*, 1543–1551. https://doi.org/10.1074/jbc.M407805200.
21. Riggins, R.B., DeBerry, R.M., Toosarvandani, M.D., and Bouton, A.H. (2003). Src-dependent association of Cas and p85 phosphatidylinositol 3'-kinase in v-crk-transformed cells. Mol. Cancer Res. *1*, 428–437.
22. Chakrabarty, A., Sánchez, V., Kuba, M.G., Rinehart, C., and Arteaga, C.L. (2012). Feedback upregulation of HER3 (ErbB3) expression and activity attenuates antitumor effect of PI3K inhibitors. Proc. Natl. Acad. Sci. USA *109*, 2718–2723. https://doi.org/10.1073/pnas.1018001108.
23. Chandarlapaty, S., Sawai, A., Scaltriti, M., Rodrik-Outmezguine, V., Grbovic-Huezo, O., Serra, V., Majumder, P.K., Baselga, J., and Rosen, N. (2011). AKT inhibition relieves feedback suppression of receptor tyrosine kinase expression and activity. Cancer Cell *19*, 58–71. https://doi.org/10.1016/j.ccr.2010.10.031.
24. Hsu, P.P., Kang, S.A., Rameseder, J., Zhang, Y., Ottina, K.A., Lim, D., Peterson, T.R., Choi, Y., Gray, N.S., Yaffe, M.B., et al. (2011). The mTOR-regulated phosphoproteome reveals a mechanism of mTORC1-mediated inhibition of growth factor signaling. Science *332*, 1317–1322. https://doi.org/10.1126/science.1199498.
25. Mukherjee, R., Vanaja, K.G., Boyer, J.A., Gadal, S., Solomon, H., Chandarlapaty, S., Levchenko, A., and Rosen, N. (2021). Regulation of

PTEN translation by PI3K signaling maintains pathway homeostasis. Mol. Cell *81*, 708–723.e5. https://doi.org/10.1016/j.molcel.2021.01.033.

26. Rodrik-Outmezguine, V.S., Chandarlapaty, S., Pagano, N.C., Poulikakos, P.I., Scaltriti, M., Moskatel, E., Baselga, J., Guichard, S., and Rosen, N. (2011). mTOR kinase inhibition causes feedback-dependent biphasic regulation of AKT signaling. Cancer Discov. *1*, 248–259. https://doi.org/10.1158/2159-8290.CD-11-0085.
27. Ebi, H., Corcoran, R.B., Singh, A., Chen, Z., Song, Y., Lifshits, E., Ryan, D.P., Meyerhardt, J.A., Benes, C., Settleman, J., et al. (2011). Receptor tyrosine kinases exert dominant control over PI3K signaling in human KRAS mutant colorectal cancers. J. Clin. Invest. *121*, 4311–4321. https://doi.org/10.1172/JCI57909.
28. Engelman, J.A., Jänne, P.A., Mermel, C., Pearlberg, J., Mukohara, T., Fleet, C., Cichowski, K., Johnson, B.E., and Cantley, L.C. (2005). ErbB-3 mediates phosphoinositide 3-kinase activity in gefitinib-sensitive non-small cell lung cancer cell lines. Proc. Natl. Acad. Sci. USA *102*, 3788–3793. https://doi.org/10.1073/pnas.0409773102.
29. Engelman, J.A., Zejnullahu, K., Mitsudomi, T., Song, Y., Hyland, C., Park, J.O., Lindeman, N., Gale, C.M., Zhao, X., Christensen, J., et al. (2007). MET amplification leads to gefitinib resistance in lung cancer by activating ERBB3 signaling. Science *316*, 1039–1043. https://doi.org/10.1126/science.1141478.
30. Stommel, J.M., Kimmelman, A.C., Ying, H., Nabioullin, R., Ponugoti, A.H., Wiedemeyer, R., Stegh, A.H., Bradner, J.E., Ligon, K.L., Brennan, C., et al. (2007). Coactivation of receptor tyrosine kinases affects the response of tumor cells to targeted therapies. Science *318*, 287–290. https://doi.org/10.1126/science.1142946.
31. Turke, A.B., Zejnullahu, K., Wu, Y.L., Song, Y., Dias-Santagata, D., Lifshits, E., Toschi, L., Rogers, A., Mok, T., Sequist, L., et al. (2010). Preexistence and clonal selection of MET amplification in EGFR mutant NSCLC. Cancer Cell *17*, 77–88. https://doi.org/10.1016/j.ccr.2009.11.022.
32. Yang, X., Turke, A.B., Qi, J., Song, Y., Rexer, B.N., Miller, T.W., Jänne, P.A., Arteaga, C.L., Cantley, L.C., Engelman, J.A., and Asara, J.M. (2011). Using tandem mass spectrometry in targeted mode to identify activators of class IA PI3K in cancer. Cancer Res. *71*, 5965–5975. https://doi.org/10.1158/0008-5472.CAN-11-0445.
33. Beckett, D., Kovaleva, E., and Schatz, P.J. (1999). A minimal peptide substrate in biotin holoenzyme synthetase-catalyzed biotinylation. Protein Sci. *8*, 921–929. https://doi.org/10.1110/ps.8.4.921.
34. Tsolakos, N., Durrant, T.N., Chessa, T., Suire, S.M., Oxley, D., Kulkarni, S., Downward, J., Perisic, O., Williams, R.L., Stephens, L., and Hawkins, P.T. (2018). Quantitation of class IA PI3Ks in mice reveals p110-free-p85s and isoform-selective subunit associations and recruitment to receptors. Proc. Natl. Acad. Sci. USA *115*, 12176–12181. https://doi.org/10.1073/pnas.1803446115.
35. Trotman, L.C., Niki, M., Dotan, Z.A., Koutcher, J.A., Di Cristofano, A., Xiao, A., Khoo, A.S., Roy-Burman, P., Greenberg, N.M., Van Dyke, T., et al. (2003). Pten dose dictates cancer progression in the prostate. PLoS Biol. *1*, E59. https://doi.org/10.1371/journal.pbio.0000059.
36. Wu, X., Wu, J., Huang, J., Powell, W.C., Zhang, J., Matusik, R.J., Sangiorgi, F.O., Maxson, R.E., Sucov, H.M., and Roy-Burman, P. (2001). Generation of a prostate epithelial cell-specific Cre transgenic mouse model for tissue-specific gene ablation. Mech. Dev. *101*, 61–69. https://doi.org/10.1016/s0925-4773(00)00551-7.
37. Jurmeister, S., Ramos-Montoya, A., Sandi, C., Pértega-Gomes, N., Wadhwa, K., Lamb, A.D., Dunning, M.J., Attig, J., Carroll, J.S., Fryer, L.G., et al. (2018). Identification of potential therapeutic targets in prostate cancer through a cross-species approach. EMBO Mol. Med. *10*, e8274. https://doi.org/10.15252/emmm.201708274.
38. Folkes, A.J., Ahmadi, K., Alderton, W.K., Alix, S., Baker, S.J., Box, G., Chuckowree, I.S., Clarke, P.A., Depledge, P., Eccles, S.A., et al. (2008). The identification of 2-(1H-indazol-4-yl)-6-(4-methanesulfonyl-piperazin-1-ylmethyl)-4-morpholin-4-yl-thieno[3,2-d]pyrimidine (GDC-0941) as a potent, selective, orally bioavailable inhibitor of class I PI3 kinase for the treatment of cancer. J. Med. Chem. *51*, 5522–5532. https://doi.org/10.1021/jm800295d.
39. Zhang, J., Kim, S., Li, L., Kemp, C.J., Jiang, C., and Lü, J. (2020). Proteomic and transcriptomic profiling of Pten gene-knockout mouse model of prostate cancer. Prostate *80*, 588–605. https://doi.org/10.1002/pros.23972.
40. Grossmann, A., Benlasfer, N., Birth, P., Hegele, A., Wachsmuth, F., Apelt, L., and Stelzl, U. (2015). Phospho-tyrosine dependent protein-protein interaction network. Mol. Syst. Biol. *11*, 794. https://doi.org/10.15252/msb.20145968.
41. Drost, J., Karthaus, W.R., Gao, D., Driehuis, E., Sawyers, C.L., Chen, Y., and Clevers, H. (2016). Organoid culture systems for prostate epithelial and cancer tissue. Nat. Protoc. *11*, 347–358. https://doi.org/10.1038/nprot.2016.006.
42. Pearson, H.B., Li, J., Meniel, V.S., Fennell, C.M., Waring, P., Montgomery, K.G., Rebello, R.J., Macpherson, A.A., Koushyar, S., Furic, L., et al. (2018). Identification of Pik3ca Mutation as a Genetic Driver of Prostate Cancer That Cooperates with Pten Loss to Accelerate Progression and Castration-Resistant Growth. Cancer Discov. *8*, 764–779. https://doi.org/10.1158/2159-8290.CD-17-0867.
43. Cancer Genome Atlas Research Network (2015). The Molecular Taxonomy of Primary Prostate Cancer. Cell *163*, 1011–1025. https://doi.org/10.1016/j.cell.2015.10.025.
44. Zhang, Y., Kwok-Shing Ng, P., Kucherlapati, M., Chen, F., Liu, Y., Tsang, Y.H., de Velasco, G., Jeong, K.J., Akbani, R., Hadjipanayis, A., et al. (2017). A Pan-Cancer Proteogenomic Atlas of PI3K/AKT/mTOR Pathway Alterations. Cancer Cell *31*, 820–832.e3. https://doi.org/10.1016/j.ccell.2017.04.013.
45. Cerami, E., Gao, J., Dogrusoz, U., Gross, B.E., Sumer, S.O., Aksoy, B.A., Jacobsen, A., Byrne, C.J., Heuer, M.L., Larsson, E., et al. (2012). The cBio cancer genomics portal: an open platform for exploring multidimensional cancer genomics data. Cancer Discov. *2*, 401–404. https://doi.org/10.1158/2159-8290.CD-12-0095.
46. Gao, J., Aksoy, B.A., Dogrusoz, U., Dresdner, G., Gross, B., Sumer, S.O., Sun, Y., Jacobsen, A., Sinha, R., Larsson, E., et al. (2013). Integrative analysis of complex cancer genomics and clinical profiles using the cBioPortal. Sci. Signal. *6*, pl1. https://doi.org/10.1126/scisignal.2004088.
47. Goldman, M.J., Craft, B., Hastie, M., Repečka, K., McDade, F., Kamath, A., Banerjee, A., Luo, Y., Rogers, D., Brooks, A.N., et al. (2020). Visualizing and interpreting cancer genomics data via the Xena platform. Nat. Biotechnol. *38*, 675–678. https://doi.org/10.1038/s41587-020-0546-8.
48. Cancer Genome Atlas Network (2012). Comprehensive molecular portraits of human breast tumours. Nature *490*, 61–70. https://doi.org/10.1038/nature11412.
49. Liu, Y., Wang, D., Li, Z., Li, X., Jin, M., Jia, N., Cui, X., Hu, G., Tang, T., and Yu, Q. (2022). Pan-cancer analysis on the role of PIK3R1 and PIK3R2 in human tumors. Sci. Rep. *12*, 5924. https://doi.org/10.1038/s41598-022-09889-0.
50. Oda, K., Stokoe, D., Taketani, Y., and McCormick, F. (2005). High frequency of coexistent mutations of PIK3CA and PTEN genes in endometrial carcinoma. Cancer Res. *65*, 10669–10673. https://doi.org/10.1158/0008-5472.CAN-05-2620.
51. Urick, M.E., Rudd, M.L., Godwin, A.K., Sgroi, D., Merino, M., and Bell, D.W. (2011). PIK3R1 (p85alpha) is somatically mutated at high frequency in primary endometrial cancer. Cancer Res. *71*, 4061–4067. https://doi.org/10.1158/0008-5472.CAN-11-0549.
52. Drake, J.M., Graham, N.A., Lee, J.K., Stoyanova, T., Faltermeier, C.M., Sud, S., Titz, B., Huang, J., Pienta, K.J., Graeber, T.G., and Witte, O.N. (2013). Metastatic castration-resistant prostate cancer reveals intrapatient similarity and interpatient heterogeneity of therapeutic kinase targets. Proc. Natl. Acad. Sci. USA *110*, E4762–E4769. https://doi.org/10.1073/pnas.1319948110.

53. Drake, J.M., Paull, E.O., Graham, N.A., Lee, J.K., Smith, B.A., Titz, B., Stoyanova, T., Faltermeier, C.M., Uzunangelov, V., Carlin, D.E., et al. (2016). Phosphoproteome Integration Reveals Patient-Specific Networks in Prostate Cancer. Cell *166*, 1041–1054. https://doi.org/10.1016/j.cell.2016.07.007.

54. Kalaany, N.Y., and Sabatini, D.M. (2009). Tumours with PI3K activation are resistant to dietary restriction. Nature *458*, 725–731. https://doi.org/10.1038/nature07782.

55. Madeira, F., Tinti, M., Murugesan, G., Berrett, E., Stafford, M., Toth, R., Cole, C., MacKintosh, C., and Barton, G.J. (2015). 14-3-3-Pred: improved methods to predict 14-3-3-binding phosphopeptides. Bioinformatics *31*, 2276–2283. https://doi.org/10.1093/bioinformatics/btv133.

56. Brummer, T., Larance, M., Herrera Abreu, M.T., Lyons, R.J., Timpson, P., Emmerich, C.H., Fleuren, E.D.G., Lehrbach, G.M., Schramek, D., Guilhaus, M., et al. (2008). Phosphorylation-dependent binding of 14-3-3 terminates signalling by the Gab2 docking protein. EMBO J. *27*, 2305–2316. https://doi.org/10.1038/emboj.2008.159.

57. Lodyga, M., De Falco, V., Bai, X.H., Kapus, A., Melillo, R.M., Santoro, M., and Liu, M. (2009). XB130, a tissue-specific adaptor protein that couples the RET/PTC oncogenic kinase to PI 3-kinase pathway. Oncogene *28*, 937–949. https://doi.org/10.1038/onc.2008.447.

58. Moodley, S., Hui Bai, X., Kapus, A., Yang, B., and Liu, M. (2015). XB130/Tks5 scaffold protein interaction regulates Src-mediated cell proliferation and survival. Mol. Biol. Cell *26*, 4492–4502. https://doi.org/10.1091/mbc.E15-07-0483.

59. Abram, C.L., Seals, D.F., Pass, I., Salinsky, D., Maurer, L., Roth, T.M., and Courtneidge, S.A. (2003). The adaptor protein fish associates with members of the ADAMs family and localizes to podosomes of Src-transformed cells. J. Biol. Chem. *278*, 16844–16851. https://doi.org/10.1074/jbc.M300267200.

60. Flynn, D.C., Leu, T.H., Reynolds, A.B., and Parsons, J.T. (1993). Identification and sequence analysis of cDNAs encoding a 110-kilodalton actin filament-associated pp60src substrate. Mol. Cell Biol. *13*, 7892–7900. https://doi.org/10.1128/mcb.13.12.7892-7900.1993.

61. Zhang, R., Zhang, J., Wu, Q., Meng, F., and Liu, C. (2016). XB130: A novel adaptor protein in cancer signal transduction. Biomed. Rep. *4*, 300–306. https://doi.org/10.3892/br.2016.588.

62. Chen, J., Wang, A., Ji, J., Zhou, K., Bu, Z., Lyu, G., and Ji, J. (2021). An Innovative Prognostic Model Based on Four Genes in Asian Patient with Gastric Cancer. Cancer Res. Treat. *53*, 148–161. https://doi.org/10.4143/crt.2020.424.

63. Deng, Z., Wang, J., Xu, B., Jin, Z., Wu, G., Zeng, J., Peng, M., Guo, Y., and Wen, Z. (2019). Mining TCGA Database for Tumor Microenvironment-Related Genes of Prognostic Value in Hepatocellular Carcinoma. BioMed Res. Int. *2019*, 2408348. https://doi.org/10.1155/2019/2408348.

64. Liu, Y., Li, C., Dong, L., Chen, X., and Fan, R. (2020). Identification and verification of three key genes associated with survival and prognosis of COAD patients via integrated bioinformatics analysis. Biosci. Rep. *40*. https://doi.org/10.1042/BSR20200141.

65. Ruiz-Deya, G., Matta, J., Encarnación-Medina, J., Ortiz-Sanchéz, C., Dutil, J., Putney, R., Berglund, A., Dhillon, J., Kim, Y., and Park, J.Y. (2021). Differential DNA Methylation in Prostate Tumors from Puerto Rican Men. Int. J. Mol. Sci. *22*, 733. https://doi.org/10.3390/ijms22020733.

66. Xing, X., Mu, N., Yuan, X., Wang, N., Juhlin, C.C., Stråat, K., Larsson, C., and Xu, D. (2020). PLEKHS1 Over-Expression is Associated with Metastases and Poor Outcomes in Papillary Thyroid Carcinoma. Cancers *12*, 2133. https://doi.org/10.3390/cancers12082133.

67. Xiong, W., Jiang, Y.X., Ai, Y.Q., Liu, S., Wu, X.R., Cui, J.G., Qin, J.Y., Liu, Y., Xia, Y.X., Ju, Y.H., et al. (2015). Microarray Analysis of Long Non-coding RNA Expression Profile Associated with 5-Fluorouracil-Based Chemoradiation Resistance in Colorectal Cancer Cells. Asian Pac. J. Cancer Prev. *16*, 3395–3402. https://doi.org/10.7314/apjcp.2015.16.8.3395.

68. Zhang, Y., Wu, X., Zhang, C., Wang, J., Fei, G., Di, X., Lu, X., Feng, L., Cheng, S., and Yang, A. (2020). Dissecting expression profiles of gastric precancerous lesions and early gastric cancer to explore crucial molecules in intestinal-type gastric cancer tumorigenesis. J. Pathol. *251*, 135–146. https://doi.org/10.1002/path.5434.

69. Abdel-Tawab, M.S., Fouad, H., Othman, A.M., Eid, R.A., Mohammed, M.A., Hassan, A., and Reyad, H.R. (2022). Evaluation of gene expression of PLEKHS1, AADAC, and CDKN3 as novel genomic markers in gastric carcinoma. PLoS One *17*, e0265184. https://doi.org/10.1371/journal.pone.0265184.

70. Weinhold, N., Jacobsen, A., Schultz, N., Sander, C., and Lee, W. (2014). Genome-wide analysis of noncoding regulatory mutations in cancer. Nat. Genet. *46*, 1160–1165. https://doi.org/10.1038/ng.3101.

71. Langenbucher, A., Bowen, D., Sakhtemani, R., Bournique, E., Wise, J.F., Zou, L., Bhagwat, A.S., Buisson, R., and Lawrence, M.S. (2021). An extended APOBEC3A mutation signature in cancer. Nat. Commun. *12*, 1602. https://doi.org/10.1038/s41467-021-21891-0.

72. Rheinbay, E., Nielsen, M.M., Abascal, F., Wala, J.A., Shapira, O., Tiao, G., Hornshøj, H., Hess, J.M., Juul, R.I., Lin, Z., et al. (2020). Analyses of non-coding somatic drivers in 2,658 cancer whole genomes. Nature *578*, 102–111. https://doi.org/10.1038/s41586-020-1965-x.

73. Vacher, S., Suybeng, V., Girard, E., Masliah Planchon, J., Thomson, G., Le Goux, C., Garinet, S., Schnitzler, A., Chemlali, W., Firlej, V., et al. (2020). Genomic Instability Signature of Palindromic Non-Coding Somatic Mutations in Bladder Cancer. Cancers *12*, 2882. https://doi.org/10.3390/cancers12102882.

74. Wong, J.K.L., Aichmüller, C., Schulze, M., Hlevnjak, M., Elgaafary, S., Lichter, P., and Zapatka, M. (2022). Association of mutation signature effectuating processes with mutation hotspots in driver genes and non-coding regions. Nat. Commun. *13*, 178. https://doi.org/10.1038/s41467-021-27792-6.

75. Fredriksson, N.J., Ny, L., Nilsson, J.A., and Larsson, E. (2014). Systematic analysis of noncoding somatic mutations and gene expression alterations across 14 tumor types. Nat. Genet. *46*, 1258–1263. https://doi.org/10.1038/ng.3141.

76. Suzuki, A., Yamaguchi, M.T., Ohteki, T., Sasaki, T., Kaisho, T., Kimura, Y., Yoshida, R., Wakeham, A., Higuchi, T., Fukumoto, M., et al. (2001). T cell-specific loss of Pten leads to defects in central and peripheral tolerance. Immunity *14*, 523–534. https://doi.org/10.1016/s1074-7613(01)00134-0.

77. Eng, J.K., McCormack, A.L., and Yates, J.R. (1994). An approach to correlate tandem mass spectral data of peptides with amino acid sequences in a protein database. J. Am. Soc. Mass Spectrom. *5*, 976–989. https://doi.org/10.1016/1044-0305(94)80016-2.

78. Stringer, C., Wang, T., Michaelos, M., and Pachitariu, M. (2021). Cellpose: a generalist algorithm for cellular segmentation. Nat. Methods *18*, 100–106. https://doi.org/10.1038/s41592-020-01018-x.

79. Liu, W., Xie, Y., Ma, J., Luo, X., Nie, P., Zuo, Z., Lahrmann, U., Zhao, Q., Zheng, Y., Zhao, Y., et al. (2015). IBS: an illustrator for the presentation and visualization of biological sequences. Bioinformatics *31*, 3359–3361. https://doi.org/10.1093/bioinformatics/btv362.

80. Perez-Riverol, Y., Bai, J., Bandla, C., García-Seisdedos, D., Hewapathirana, S., Kamatchinathan, S., Kundu, D.J., Prakash, A., Frericks-Zipper, A., Eisenacher, M., et al. (2022). The PRIDE database resources in 2022: a hub for mass spectrometry-based proteomics evidences. Nucleic Acids Res. *50*, D543–D552. https://doi.org/10.1093/nar/gkab1038.

81. Kofuji, S., Kimura, H., Nakanishi, H., Nanjo, H., Takasuga, S., Liu, H., Eguchi, S., Nakamura, R., Itoh, R., Ueno, N., et al. (2015). INPP4B Is a PtdIns(3,4,5)P3 Phosphatase That Can Act as a Tumor Suppressor. Cancer Discov. *5*, 730–739. https://doi.org/10.1158/2159-8290.CD-14-1329.

82. Leneuve, P., Colnot, S., Hamard, G., Francis, F., Niwa-Kawakita, M., Giovannini, M., and Holzenberger, M. (2003). Cre-mediated germline mosaicism: a new transgenic mouse for the selective removal of residual

markers from tri-lox conditional alleles. Nucleic Acids Res. *31*, e21. https://doi.org/10.1093/nar/gng021.

83. Yang, W., Hosford, S.R., Dillon, L.M., Shee, K., Liu, S.C., Bean, J.R., Salphati, L., Pang, J., Zhang, X., Nannini, M.A., et al. (2016). Strategically Timing Inhibition of Phosphatidylinositol 3-Kinase to Maximize Therapeutic Index in Estrogen Receptor Alpha-Positive, PIK3CA-Mutant Breast Cancer. Clin. Cancer Res. *22*, 2250–2260. https://doi.org/10.1158/1078-0432.CCR-15-2276.

84. Karthaus, W.R., Iaquinta, P.J., Drost, J., Gracanin, A., van Boxtel, R., Wongvipat, J., Dowling, C.M., Gao, D., Begthel, H., Sachs, N., et al. (2014). Identification of multipotent luminal progenitor cells in human prostate organoid cultures. Cell *159*, 163–175. https://doi.org/10.1016/j.cell.2014.08.017.

85. Luff, D.H., Wojdyla, K., Oxley, D., Chessa, T., Hudson, K., Hawkins, P.T., Stephens, L.R., Barry, S.T., and Okkenhaug, K. (2021). PI3Kdelta Forms Distinct Multiprotein Complexes at the TCR Signalosome in Naive and Differentiated CD4(+) T Cells. Front. Immunol. *12*, 631271. https://doi.org/10.3389/fimmu.2021.631271.

86. Köhler, G., and Milstein, C. (1975). Continuous cultures of fused cells secreting antibody of predefined specificity. Nature *256*, 495–497. https://doi.org/10.1038/256495a0.

87. Rynkiewicz, N.K., Anderson, K.E., Suire, S., Collins, D.M., Karanasios, E., Vadas, O., Williams, R., Oxley, D., Clark, J., Stephens, L.R., and Hawkins, P.T. (2020). Gbetagamma is a direct regulator of endogenous p101/p110gamma and p84/p110gamma PI3Kgamma complexes in mouse neutrophils. Sci. Signal. *13*, eaaz4003. https://doi.org/10.1126/scisignal.aaz4003.

88. Clark, J., Anderson, K.E., Juvin, V., Smith, T.S., Karpe, F., Wakelam, M.J.O., Stephens, L.R., and Hawkins, P.T. (2011). Quantification of PtdInsP3 molecular species in cells and tissues by mass spectrometry. Nat. Methods *8*, 267–272. https://doi.org/10.1038/nmeth.1564.

89. Stephens, L.R., Anderson, K.E., and Hawkins, P.T. (2001). Src family kinases mediate receptor-stimulated, phosphoinositide 3-kinase-dependent, tyrosine phosphorylation of dual adaptor for phosphotyrosine and 3-phosphoinositides-1 in endothelial and B cell lines. J. Biol. Chem. *276*, 42767–42773. https://doi.org/10.1074/jbc.M107194200.

Please cite this article in press as: Chessa et al., PLEKHS1 drives PI3Ks and remodels pathway homeostasis in PTEN-null prostate, Molecular Cell (2023), https://doi.org/10.1016/j.molcel.2023.07.015

STAR★METHODS

KEY RESOURCES TABLE

REAGENT or RESOURCE	SOURCE	IDENTIFIER
Antibodies		
Mouse Anti-Akt, phospho (Thr308) Monoclonal Antibody, Unconjugated, Clone L32A4	Cell Signaling Technology	Cat# 5106, RRID:AB_836861
Phospho-Akt (Ser473) Antibody	Cat# 9271,	Cell Signaling Technology RRID:AB_329825
Akt Antibody	Cell Signaling Technology	Cat# 9272, RRID:AB_329827
Phospho-p70 S6 Kinase (Thr389) Antibody	Cell Signaling Technology	Cat# 9205, RRID:AB_330944
IRS-1 Antibody	Cell Signaling Technology	Cat# 2382, RRID:AB_330333
IRS-1 (59G8) Rabbit mAb (Figure S5H)	Cell Signaling Technology	Cat# 2390, RRID:AB_10692516
Insulin Receptor beta (4B8) Rabbit mAb antibody	Cell Signaling Technology	Cat# 3025, RRID:AB_2280448
IGF-I Receptor (D23H3) XP Rabbit mAb antibody	Cell Signaling Technology	Cat# 9750, RRID:AB_10950969
Phospho-GSK-3alpha/beta (Ser21/9) Antibody	Cell Signaling Technology	Cat# 9331, RRID:AB_329830
Phospho-p44/42 MAPK (Erk1/2) (Thr202/Tyr204) (E10) Mouse mAb antibody	Cell Signaling Technology	Cat# 9106, RRID:AB_331768
Anti-p38 MAPK, phospho (Thr180/Tyr182) Antibody, Unconjugated	Cell Signaling Technology	Cat# 9211, RRID:AB_331641
Anti-p38 MAPK Antibody, Unconjugated	Cell Signaling Technology	Cat# 9212, RRID:AB_330713
PI3 Kinase p85 Antibody	Cell Signaling Technology	Cat# 4292, RRID:AB_329869
PI3 Kinase p110alpha (C73F8) Rabbit mAb	Cell Signaling Technology	Cat# 4249, RRID:AB_2165248
PI3 Kinase p110β (C33D4) Rabbit mAb	Cell Signaling Technology	Cat# 3011, RRID:AB_2165246
PTEN (D4.3) XP Rabbit mAb	Cell Signaling Technology	Cat# 9188, RRID:AB_2253290
Phospho-Src Family (Tyr416) (D49G4) Rabbit mAb	Cell Signaling Technology	Cat# 6943, RRID:AB_10013641
Anti-rabbit IgG, HRP-linked Antibody	Cell Signaling Technology	Cat# 7074, RRID:AB_2099233
Rabbit Anti-Mouse IgG (Light Chain Specific) (D3V2A) mAb (HRP Conjugate)	Cell Signaling Technology	Cat# 58802, RRID:AB_2799549
PI 3-kinase p110delta (H-219)	Santa Cruz Biotechnology	Cat# sc-7176, RRID:AB_2165540
PLEKHS1 antibody 9930023K05Rik (G-17)	Santa Cruz Biotechnology	Cat# sc-240003, RRID:AB_10842269
PLEKHS1 antibody 9930023K05Rik (M-16)	Santa Cruz Biotechnology	Cat# sc-240005, RRID:AB_10851029
PI 3-kinase p55gamma (E−9)	Santa Cruz Biotechnology	Cat# sc-376615, RRID:AB_11150683
PI3K p85 alpha Monoclonal Antibody (U13)	Thermo Fisher Scientific	Cat# MA1-21472, RRID:AB_2299554
Goat anti-Rabbit IgG (H + L) Highly Cross-Adsorbed Secondary Antibody, Alexa Fluor™ 488	Thermo Fisher Scientific	Cat# A-11034, RRID:AB_2576217
AFAP1L2 antibody	Proteintech	Cat# 17183-1-AP, RRID:AB_2226101
4G10® Platinum, Anti-Phosphotyrosine Antibody (mouse monoclonal cocktail IgG2b)	Millipore	Cat# 05–1050, RRID:AB_916371
4G10 Platinum, Anti-Phosphotyrosine, Agarose Conjugate antibody	Millipore	Cat# 16–638, RRID:AB_11212502
Anti-GFP	Sigma-Aldrich	Cat# 11814460001, RRID:AB_390913
Avi-tag antibody	GenScript	Cat# A00674, RRID:AB_915553

(*Continued on next page*)

Please cite this article in press as: Chessa et al., PLEKHS1 drives PI3Ks and remodels pathway homeostasis in PTEN-null prostate, Molecular Cell (2023), https://doi.org/10.1016/j.molcel.2023.07.015

CellPress
OPEN ACCESS

Continued

REAGENT or RESOURCE	SOURCE	IDENTIFIER
βCOP mouse monoclonal antibody	kind gift from Dr N. Ktistakis, Signaling Department, Babraham Institute	N/A
Goat Anti-Mouse IgG (H L)-HRP Conjugate	Bio-Rad	Cat# 170–6516, RRID:AB_11125547
Goat Anti-Rabbit IgG (H L)-HRP Conjugate	Bio-Rad	Cat# 172–1019, RRID:AB_11125143
Cytokeratin 8 antibody [EP1628Y]	Abcam	Cat# ab53280, RRID:AB_869901
Src antibody [Clone 327]	Abcam	Cat# ab16885, RRID:AB_443522
Donkey polyclonal Secondary Antibody to Goat IgG - H&L (HRP)	Abcam	Cat# ab97110, RRID:AB_10679463
VeriBlot for IP Detection Reagent (HRP)	Abcam	Cat# ab131366, RRID:AB_2892718
CD326/EpCAM-FITC	BioLegend	118207
CD49f-PE	Miltenyi Biotec	130-100-096
Avi-tag mouse monoclonal antibody	Babraham Bioscience Technologies (BBT)/ BRC technology development lab	Custom-made
Anti-mouse phospho-Y258-PLEKHS1 antibody (rabbit pAb)	Cambridge Research Biochemicals	Custom-made
Anti-human PLEKHS1 antibody (rabbit pAb)	Cambridge Research Biochemicals	Custom-made
Bacterial and virus strains		
BL21-CodonPlus (DE3)-RIPL Competent Cells	Agilent Technologies	230280
Biological samples		
Mouse prostate tissue of the indicated genotypes	Trotman, L. C. et al.,[35] this paper, Pearson et al.[42]	N/A
Mouse ovary tissue of the indicated genotypes	European Mouse Mutant Archive (EMMA), Suzuki et al.,[76] this paper	N/A
Mouse prostate organoids of the indicated genotypes	This paper	N/A
Chemicals, peptides, and recombinant proteins		
TMS-diazomethane	Sigma-Aldrich	362832
Tris	Melford	B2005
NaCl	VWR Chemicals	27810.295
EDTA	Sigma-Aldrich	E5134
EGTA	Sigma-Aldrich	E4378
Triton X-100	Sigma-Aldrich	T9284
CHAPS hydrate	Sigma-Aldrich	C3023
Nonidet P40 Substitute	Roche	11754599001
Sodium deoxycholate	Sigma-Aldrich	D6750
SDS (Sodium Dodecyl Sulfate)	Bio-Rad	1610301
Anti-protease leupeptin	Sigma-Aldrich	L8511
Anti-protease aprotinin	Sigma-Aldrich	A1153
Anti-protease antipain	Sigma-Aldrich	A6191
Anti-protease pepstatin A	Sigma-Aldrich	P5318
PMSF	Sigma-Aldrich	78830
$Na_4P_2O_7$	Sigma-Aldrich	P8010
β-glycerophosphate	Calbiochem	35675
Na_3VO_4	Sigma-Aldrich	S6508
NaF	Sigma-Aldrich	S7920
Dynabeads™ M-280 Streptavidin	Thermo Fisher Scientific	11205D
Dynabeads™ Protein G for Immunoprecipitation	Thermo Fisher Scientific	10003D
PVDF membranes (Immobilon P)	Millipore	IPVH00010

(*Continued on next page*)

Please cite this article in press as: Chessa et al., PLEKHS1 drives PI3Ks and remodels pathway homeostasis in PTEN-null prostate, Molecular Cell (2023), https://doi.org/10.1016/j.molcel.2023.07.015

Continued

REAGENT or RESOURCE	SOURCE	IDENTIFIER
TWEEN® 20	Sigma-Aldrich	P1379
ECL™ Western Blotting Reagents Cytiva RPN2106	Merck	GERPN2106
DTT	Melford	MB1015
Tris-HCl	Sigma-Aldrich	T3253
Glycerol	Invitrogen	15514–011
Bromophenol Blue	Sigma-Aldrich	B8026
HCl 37%	VWR	20252.335
Methanol	Romil	H410
Chloroform	Romil	H140
Ammonium acetate	Sigma-Aldrich	A1542
GDC-0941/Pictisilib	Cell Guidance Systems	SM19
Polysorbate 80	Sigma-Aldrich	W291706
Methocel	Colorcon	K4M Premium ID34516
Paraformaldehyde; powder	Sigma-Aldrich	P6148
Embedding medium	Thermo Scientific	1310
Mayer's hematoxylin solution	Sigma-Aldrich	SLBP6175V
Eosin Y solution	Sigma-Aldrich	SLBP1949V
Hoechst 33342 powder	Fluka	14533
TO-PRO3	Thermo Fisher Scientific	T3605
Horse serum	PAA	B15-020
Bovine Serum Albumin; fatty acid free, low endotoxin	Sigma-Aldrich	A8806
Vectashield	Vector Laboratories	H-1000
VECTASHIELD containing DAPI	Vector Laboratories	H-1200
RPMI 1640 Medium, GlutaMAX™ Supplement (Gibco)	Thermo Fisher Scientific	61870–010
FBS, qualified, heat inactivated, US origin (Gibco)	Thermo Fisher Scientific	16140–071
Penicillin/streptomycin	Life Technologies	15140–122
Recombinant Human R-Spondin-1	Peprotech	120–38
Recombinant Murine Noggin	Peprotech	250–38
Y-27632 dihydrochloride $\geq$98% (HPLC)	Sigma-Aldrich	Y0503
5α-Dihydrotestosterone (DHT) solution 1.0 mg/mL in methanol	Sigma-Aldrich	D-073
Trypsin-EDTA (0.25%), phenol red	Thermo Fisher Scientific/Gibco	25200–056
Nunc® Lab-Tek® II Chamber Slide™ system; 4-well	Thermo Scientific	154526
N-acetyl-L-cysteine, BioReagent, suitable for cell culture	Sigma	A9165
GlutaMAX™ Supplement	Thermo Fisher Scientific/Gibco	35050–061
Collagenase, Type II	Thermo Fisher Scientific/Gibco	17101–015
EGF, murine, suitable for cell culture	Sigma	E4127
A-8301	R&D Systems	2939
HEPES solution, 1 M, pH 7.0–7.6, sterile-filtered, BioReagent, suitable for cell culture	Sigma	H0887-100ML
B-27® Supplement (50X), minus vitamin A	Thermo Fisher Scientific	12587010
Advanced DMEM/F-12	Thermo Fisher Scientific	12634–010
Corning® Matrigel® Growth Factor Reduced (GFR) Basement Membrane Matrix, phenol red-free	VWR	734–1101

(*Continued on next page*)

Please cite this article in press as: Chessa et al., PLEKHS1 drives PI3Ks and remodels pathway homeostasis in PTEN-null prostate, Molecular Cell (2023), https://doi.org/10.1016/j.molcel.2023.07.015

Continued

REAGENT or RESOURCE	SOURCE	IDENTIFIER
Lipofectamine™ 3000 Transfection Reagent	Thermo Fisher Scientific	L3000001
ChromoTek GFP-Trap® magnetic agarose	Proteintech	gtma-100
4–15% Mini-PROTEAN® TGX™ Precast Protein Gels, 50 μL	Bio-Rad	#4561084
TRIzol™ Reagent	Thermo Fisher Scientific	15596026
Invitrogen™ SuperScript™ II Reverse Transcriptase	Thermo Fisher Scientific	18064014
Random Hexamer Primers	Thermo Fisher Scientific	SO142
Na/HPO4	BDH	102454
imidazole	Sigma-Aldrich	I5513
PD10 columns	Cytiva	17–0851
NaOH	Fisher	S/4920/53
6xHis-tagged-Tobacco Etch Virus (TEV)-protease	Thermo Fisher Scientific	T4455
Co2+ affinity resin	Thermo Fisher Scientific	89964
MBP-TRAPTM HP	Cytiva	29–0486
D(+)Maltose	Sigma-Aldrich	63418
Centricon Ultracel YM-50 Amicon	Millipore	4224
BSA	Sigma	7906
Coomassie Brilliant Blue G	Sigma-Aldrich	B1131
Imperial™ Protein Stain	Thermo Fisher Scientific	24615
HEPES	Sigma-Aldrich	H3375
Halt™ Protease Inhibitor Cocktail (100X)	Thermo Fisher Scientific	78429
HisPur™ Cobalt Resin	Thermo Fisher Scientific	89965
PIP StripsTM	Echelon Biosciences	P-6001
PIP Array	Echelon Biosciences	P-6100
Phosphatidylserine	Sigma Aldrich	840032C
Phosphatidylcholine	Sigma Aldrich	840051C
Phosphatidylethanolamine	Merck	Y0001953
sphingomyelin	Sigma Aldrich	860062P
C17:0/C16:0-PI	Synthesized by the Biological Chemistry Department in Babraham Institute	N/A
C18:0/C20:4-PI(4,5)P_2	Synthesized by the Biological Chemistry Department in Babraham Institute	N/A
N/AC18:0/C20:4-PI(3,4,5)P_3	Synthesized by the Biological Chemistry Department in Babraham Institute	N/A
Sep-Pak aminopropyl anion-exchange cartridge	Waters	WAT023610, 100-mg sorbent
sucrose	Fisher	1010099
KCl	VWR	26764.260
$CaCl_2$	Fisher	1010099
$MgCl_2$	VWR	25108.295
TrypLE™ Express Enzyme (1X), no phenol red	Thermo Fisher Scientific	12604013
Critical commercial assays		
TMTsixplex™ Isobaric Label Reagent Set	Thermo Fisher Scientific	90066
TMT10plex Isobaric Label Reagent Set plus TMT11-131C Label Reagent	Thermo Fisher Scientific	A37725
Pierce™ BCA Protein Assay Kit	Thermo Fisher Scientific	23225

(*Continued on next page*)

Please cite this article in press as: Chessa et al., PLEKHS1 drives PI3Ks and remodels pathway homeostasis in PTEN-null prostate, Molecular Cell (2023), https://doi.org/10.1016/j.molcel.2023.07.015

Continued

REAGENT or RESOURCE	SOURCE	IDENTIFIER
Bio-Rad Protein Assay Dye Reagent Concentrate	Bio-Rad	5000006
Quikchange Lightning Site-directed Mutagenesis kit	Agilent	210518
Q5® Site-Directed Mutagenesis Kit	New England Biolabs	E0554S
Deposited data		
Gene expression data (RNAseq)	NCBI Gene Expression Omnibus	GSE94574
LC-MS/MS data	ProteomeXChange	PXD043239
Original Images deposited at Mendeley Data	Mendeley Data	https://doi.org/10.17632/6z68wjh2cc.1
Experimental models: Cell lines		
LNCaP	ATCC	CRL 1740
Experimental models: Organisms/strains		
PbCre4^{+} mice	JAX	Strain 026662
Pten$^{loxP/loxP}$ mice	Trotman, L. C. et al.[35]	N/A
p85$^{WT/WT}$ x *Pten*$^{WT/WT}$ mice (*PbCre4*$^{-}$ x *mBirA*$^{+/-}$ x *Pten*$^{loxP/loxP}$)	This paper	N/A
p85α$^{Avi/Avi}$ *x Pten*$^{WT/WT}$ (*PbCre4*$^{-}$ x *Pik3r1*$^{Avi/Avi}$ x *mBirA*$^{+/-}$ x *Pten*$^{loxP/loxP}$) mice	This paper	N/A
p85β$^{Avi/Avi}$ *x Pten*$^{WT/WT}$ (*PbCre4*$^{-}$ x *Pik3r2*$^{Avi/Avi}$ x *mBirA*$^{+/-}$ x *Pten*$^{loxP/loxP}$)	This paper	N/A
p85$^{WT/WT}$ *x Pten*$^{-/-}$ (*PbCre4*$^{+}$ x *mBirA*$^{+/-}$ x *Pten*$^{loxP/loxP}$)	This paper	N/A
p85α$^{Avi/Avi}$ *x Pten*$^{-/-}$ (*PbCre4*$^{+}$ x *Pik3r1*$^{Avi/Avi}$ x *mBirA*$^{+/-}$ x *Pten*$^{loxP/loxP}$)	This paper	N/A
p85β$^{Avi/Avi}$ *x Pten*$^{-/-}$ (*PbCre4*$^{+}$ x *Pik3r2*$^{Avi/Avi}$ x *mBirA*$^{+/-}$ x *Pten*$^{loxP/loxP}$)	This paper	N/A
Plekhs1$^{Avi/Avi}$ mice and relevant crosses with *PbCre4*$^{-}$ x *mBirA*$^{+/-}$ x *Pten*$^{loxP/loxP}$ mice and *PbCre4*$^{+}$ x *mBirA*$^{+/-}$ x *Pten*$^{loxP/loxP}$ mice	This paper	N/A
Plekhs1$^{-/-}$ mice and relevant crosses with *Pten*$^{loxP/loxP}$ mice and *PbCre4*$^{+}$ x *Pten*$^{loxP/loxP}$ mice	This paper	ESC clones: Eucomm (Clone IDs HEPDO817_1_F11, HEPDo817_1_D12; Allele Plekhs1tm2a(EUCOMM)Hmgu)
PBiCre$^{+/-}$*;Pik3ca*$^{+/+}$, *Pik3ca*$^{+/HR}$ *(PBiCre*$^{+/-}$*;Pik3ca*$^{+/Lat-H1047R}$*) and Pten*$^{fl/fl}$ *(PBiCre*$^{+/-}$*;Pten*$^{fl/fl}$*) mice*	Pearson et al.[42]	N/A
Cd11b-Cre mice	European Mouse Mutant Archive (EMMA)	Tg(ITGAM-cre)2781Gkl
Pten$^{loxP/loxP}$	Suzuki et al.[76]	N/A
Ship2$^{loxP/loxP}$	This paper	N/A
Oligonucleotides		
Cloning of m*Plekhs1* iPH into pRSET-mEGFP. Forward primer: CCGATTC ATATGGGCAAACAATTTACATTTG ATTATGAAAATGAAGTCC Reverse primer: GCTACCGCCGG ATCCACCCTGGCAGTATGGTGTC	Sigma-Aldrich	N/A
Cloning of full length m*Plekhs1* (10–459) into pRSET-mEGFP: Forward primer CCGAT TCATATGGGCAAACAATTTACTTTGATTA TGAAAATGAAGTCC Reverse primer AATCGGGGTACCCTCCCCAGCAGCT TCCTTC	Sigma-Aldrich	N/A

(*Continued on next page*)

Continued

REAGENT or RESOURCE	SOURCE	IDENTIFIER
Generating 2x(10 His)MBP-mEGFP (pRSET-mEGFP) empty vector: Forward primer: AAGAGAGACATATGG TGAGCAAGGGC Reverse primer: AAGA GAGAAAGCTTTTACTTGTACAGCTCG	Sigma-Aldrich	N/A
Cloning of full length m*Plekhs1* into pCMV3-EE: Forward primer: CCGATTGCGGCC GCCCATGGAAGCCAGACCTCCAAAA GGCCCAGGCAAACAATTTACATTTGA TTATGAAAATGAAGTCC Reverse primer: GCTACCGCCTC TAGATTACTTGTACAGCTCGTCCATGC	Sigma-Aldrich	N/A
Generating pCMV3-EE-mEGFP: Forward primer: CCGATTGCGGCCG CCCATGGTGAGCAAGGGCG Reverse primer: GCTACCGCCTCT AGATTACTTGTACAGCTCGTCCATGC	Sigma-Aldrich	N/A
Recombinant DNA		
pRSET-mEGFP	This paper	N/A
pRSET-mPLEKHS1-mEGFP	This paper	N/A
pRSET-mPLEKHS1-iPH-mEGFP	This paper	N/A
pCMV3-EE-mEGFP	This paper	N/A
pCMV3-EE-mPLEKHS1-mEGFP	This paper	N/A
pCMV3-EE-mPLEKHS1-Y257F-mEGFP	This paper	N/A
pCMV3-EE-mPLEKHS1-ΔPH-mEGFP	This paper	N/A
pLNCX	This paper	N/A
pLNCX chick src Y527F	Addgene	Addgene_13660
pLNCX chick src K295R	Addgene	Addgene_13659
Software and algorithms		
Guide RNA Design Tool	Benchling; www.benchling.com	N/A
Proteome Discoverer	Thermo Fisher Scientific	N/A
SEQUEST	Eng et al.[77]	N/A
Skyline software	Washington University	N/A
Image Studio Lite v.5.2.	Licor	N/A
AxioVision	Zeiss	N/A
Napari	Napari, Python	N/A
Cellpose plugin; cellpose.org	Stringer et al.[78]	N/A
cBioPortal for cancer genomics	cBioPortal	N/A
Prism	GraphPad	N/A
ggplot2, R	R	N/A
FlowJo	BD Biosciences	N/A
Other		
Schematics and diagrams in Figures 1, 2, 7, and S6	BioRender; https://app.biorender.com/	N/A
Protein domain map in Figure 3A	IBS.http://ibs.biocuckoo.org/(Liu et al.[79])	N/A
Schematic in Figure S3C	Benchling; www.benchling.com	N/A

RESOURCE AVAILABILITY

Lead contact

Further information and requests for resources and reagents should be directed to and will be fulfilled by the lead contact, Len Stephens, len.stephens@babraham.ac.uk, the Babraham Institute, Cambridge, CB22 3AT, UK.

Materials availability

Plasmids and mouse models generated in this study will be made available upon request.

Data and code availability

- The majority of data generated and analyzed by this study are included in the published article and its supplemental information files. Original Western blot and microscopy images are deposited at Mendeley and are publicly available as of the date of publication. The DOI is listed in the key resources table. The mass spectrometry proteomics data have been deposited to the ProteomeXchange Consortium via the PRIDE[80] partner repository with the dataset identifier PXD043239. RNAseq data have been deposited to NCBI Gene Expression Omnibus (GEO) under the accession code GSE94574. All data are publicly available as of the date of publication. Accession numbers and DOI are listed in the key resources table.
- This paper does not report original code.
- Any additional information required to reanalyse the data reported in this paper is available from the lead contact upon request.

EXPERIMENTAL MODEL AND STUDY PARTICIPANT DETAILS

Experimental animals

Pik3r1$^{Avi/Avi}$, *Pik3r2*$^{Avi/Avi}$ and *mBirA*$^{+/+}$ mice[34] were bred with *PbCre4*$^{+}$ mice[36] and *Pten*$^{loxP/loxP}$ mice[35] to generate

p85$^{w/w}$ x *Pten*$^{WT/WT}$ (*PbCre4*$^{-}$ x *mBirA*$^{+/-}$ x *Pten*$^{loxP/loxP}$),
p85α$^{Avi/Avi}$ x *Pten*$^{WT/WT}$ (*PbCre4*$^{-}$ x *Pik3r1*$^{Avi/Avi}$ x *mBirA*$^{+/-}$ x *Pten*$^{loxP/loxP}$),
p85β$^{Avi/Avi}$ x *Pten*$^{WT/WT}$ (*PbCre4*$^{-}$ x *Pik3r2*$^{Avi/Avi}$ x *mBirA*$^{+/-}$ x *Pten*$^{loxP/loxP}$),
p85$^{w/w}$ x *Pten*$^{-/-}$ (*PbCre4*$^{+}$ x *mBirA*$^{+/-}$ x *Pten*$^{loxP/loxP}$),
p85α$^{Avi/Avi}$ x *Pten*$^{-/-}$ (*PbCre4*$^{+}$ x *Pik3r1*$^{Avi/Avi}$ x *mBirA*$^{+/-}$ x *Pten*$^{loxP/loxP}$),
p85β$^{Avi/Avi}$ x *Pten*$^{-/-}$ (*PbCre4*$^{+}$ x *Pik3r2*$^{Avi/Avi}$ x *mBirA*$^{+/-}$ x *Pten*$^{loxP/loxP}$).

Resulting mice were backcrossed to the C57BL/6J strain for at least 4 generations. For breeding, only *PbCre4*$^{+}$ males were used.

Plekhs1$^{Avi/Avi}$ mice were generated in BIfacilities using CRISPR/Cas9 technology. gRNAs were designed with the Guide RNA Design Tool (www.benchling.com). Zygotes used to generate *Plekhs1*$^{Avi/Avi}$ mice were isolated from *Pten*$^{loxP/loxP}$, *BirA*$^{+/+}$ females and then transferred to a WT C57BL/6J foster mother. Mice were bred with *PbCre4*$^{+}$, *Pten*$^{loxP/loxP}$ mice to generate PLEKHS1-Avi x *Pten*$^{WT/WT}$ (*PbCre4*$^{-}$ x *Plekhs1*$^{Avi/Avi}$ x *mBirA*$^{+/-}$ x *Pten*$^{loxP/loxP}$), PLEKHS1-Avi x *Pten*$^{-/-}$ (*PbCre4*$^{+}$ x *Plekhs1*$^{Avi/Avi}$ x *mBirA*$^{+/-}$ x *Pten*$^{loxP/loxP}$) mice and their appropriate no-Avi controls.

Plekhs1$^{-/-}$ mice were generated using two genetically engineered embryonic stem cells clones purchased from Eucomm (Clone IDs HEPDO817_1_F11, HEPDo817_1_D12; Allele *Plekhs1*$^{tm2a(EUCOMM)Hmgu}$) injected to a zygote isolated from *Pten*$^{loxP/loxP}$ females and then transferred to a WT C57BL/6J foster mother. Mice were bred with *Pten*$^{loxP/loxP}$ mice and *PbCre4*$^{+}$, *Pten*$^{loxP/loxP}$ mice to generate *Plekhs1*$^{w/w}$ x *Pten*$^{WT/WT}$, *Plekhs1*$^{+/-}$ x *PTEN*$^{WT/WT}$, *Plekhs1*$^{-/-}$ x *Pten*$^{WT/WT}$, *Plekhs1*$^{w/w}$ x *Pten*$^{-/-}$, *Plekhs1*$^{+/-}$ x *PTEN*$^{-/-}$ and *Plekhs1*$^{-/-}$ x *Pten*$^{-/-}$ mice.

PBiCre$^{+/-}$*;Pik3ca*$^{+/+}$, *Pik3ca*$^{+/HR}$ (*PBiCre*$^{+/-}$*;Pik3ca*$^{+/Lat-H1047R}$) and *Pten*$^{fl/fl}$ (*PBiCre*$^{+/-}$*;Pten*$^{fl/fl}$) mice were maintained on a pure FVB/NJ genetic background, and have been previously described.[42]

Ship2/Inppl1 was conditionally targeted by the methods described in our previous paper.[81] Briefly, the targeting vector was constructed to delete a genomic fragment containing the 13th to 19th exons of the mouse *Ship2/Inppl1* gene encoding the phosphatase domain by homologous recombination in E14K mouse embryonic stem cells and the resultant mutant embryonic stem cells were injected into C57BL/6J blastocysts (CLEA Japan). Chimeric male mice were crossed with C57BL/6J females to achieve germline transmission. Deletion of the LacZ-PGK- Neo^{r} cassette to generate *Ship2*$^{+/loxP}$ mice was achieved by crossing to MeuCre40 transgenic mice.[82] *Ship2*$^{+/loxP}$ mice, *Pten*$^{+/loxP}$ mice[76] and *Cd11b-Cre* mice (Strain Tg(ITGAM-cre)2781Gkl from EMMA) were bred to generate *Pten*$^{loxP/loxP}$ x *Ship2*$^{loxP/loxP}$ *x Cd11b-Cre mice.*

Experimental procedures

To determine effects of the pan-PI3K inhibitor GDC-0941 on levels of PIP_3, p85-PLEKHS1 interactions, PLEKHS1 phosphorylation and growth factor signaling *in vivo* we treated *p85α*$^{Avi/Avi}$ *x Pten*$^{WT/WT}$, *p85α*$^{Avi/Avi}$ *x Pten*$^{-/-}$, PLEKHS1-Avi x *Pten*$^{WT/WT}$ (*PbCre4*$^{-}$ x *Plekhs1*$^{Avi/Avi}$ x *mBirA*$^{+/-}$ x *Pten*$^{loxP/loxP}$) and PLEKHS1-Avi x *Pten*$^{-/-}$ mice with 800 mg/kg GDC-0941 formulated in HPMC/Tween [0.5% hydroxypropyl methocellulose (Methocel (Colorcon))/0.2% Polysorbate80] or vehicle p.o. once daily, for 2 days. Animals were sacrificed between 2 and 5 h after administration of the last dose, at which plasma concentration of GDC-0941 was expected to be between 5 and 10 μM.[83]

Ethical statement

All animal experiments at The Babraham Institute were reviewed and approved by The Animal Welfare and Ethics Review Body and performed under Home Office Project license PPL 70/8100 or by the Institutional Animal Care and Use Committee of the Tokyo Medical and Dental University (ID: A2023-002A).

Please cite this article in press as: Chessa et al., PLEKHS1 drives PI3Ks and remodels pathway homeostasis in PTEN-null prostate, Molecular Cell (2023), https://doi.org/10.1016/j.molcel.2023.07.015

CellPress
OPEN ACCESS

Housing and husbandry

All animals used in this study were housed in the Biological Support Unit at the Babraham Institute and kept under specific pathogen–free conditions. Animals housed in the Biological Support Unit at the Babraham Institute were kept under specific pathogen–free conditions.

Pten$^{loxP/loxP}$ x Ship2$^{loxP/loxP}$ *x Cd11b-Cre and their founder* mice were maintained under specific pathogen-free conditions at Tokyo Medical and Dental University, and female 12- to 28-week-old mice were used.

Animal care and monitoring

The animals were kept under SPF conditions and the animal facilities where the mice were kept were regularly checked for standard pathogens. The mice were looked after by professional caretakers. Every animal was checked daily. Health reports can be provided upon request.

Food and water were provided *ad libitum*. The light cycle ran from 6 a.m. to 6 p.m.

Study design, sample size and Randomisation

Prostates from male mice and ovaries from female mice, from several age-matched mice of identical genotype, randomly allocated to different experimental groups, were analyzed, as detailed in the legends to figures. Multiple independent experiments were carried out using several biological replicates, as detailed in the legends to figures.

Cell lines

LNCaP

LNCaP cells (male) were obtained from the AstraZeneca cell bank and had been previously authenticated using DNA fingerprinting short tandem repeat assays. Cells were cultured in RPMI-1640 supplemented with 10% FBS and 1% w/v penicillin/streptomycin, for a maximum of 25 passages post-thaw.

Organoid culture

Prostate cell isolation and subsequent organoid culture was performed according to methodology described by Karthaus et al.[84] For organoid culture maintenance, cells derived from dorsolateral prostate (DLP) lobes were cultured by overlaying 10000 cells, in 400 μL full organoid growth medium (ADMEM/F12 supplemented with 10 mM HEPES pH 7.4, 2 mM Glutamax and 1x Penicillin-Streptomycin, as well as additional components B27 minus vitamin A, N-acetyl-L-cysteine (1.25 mM), murine EGF (50 ng/mL), recombinant murine Noggin (100 ng/mL), recombinant human R-Spondin-1 (500 ng/mL), Y-27632 dihydrochloride (10 μM), 5α-Dihydrotestosterone (DHT) solution (1 nM) and A 83-01 (200 nM), onto 95 μL Corning Matrigel Growth Factor Reduced (GFR) Basement Membrane Matrix, in a Nunc LabTek II chamber slide system (4-well; glass).

For PIP_3 measurements, 5000 cells (Figure 6G) or 2500 cells (Figure 6H) in 200 μL full organoid growth medium were cultured in 96-well plates containing 47.5 μL growth factor-reduced Matrigel for 4 days. Organoids were treated with vehicle (DMSO; 0.11%) or SFK-inhibitors A-419259 (1μM) and PP2 (10 μM) for 2 h at 37◦C (Figure 6H). Organoids were cultured for a maximum of 8 passages in complete ADMEM/F12 medium (Figures 6G and S5F) or for 0 passages in complete ADMEM/F12 medium (Figures 6H, 6I, S5E, and S5G).

For transmitted light imaging, 2500 cells in 200 μL complete ADMEM/F12 medium were cultured in 96-well plates for 4 days 24 h after plating, complete ADMEM/F12 medium was replaced with medium containing vehicle (DMSO; 0.11%) or SFK-inhibitors A-419259 (1μM) and PP2 (10 μM). Medium was replaced every day with fresh medium with vehicle or inhibitors. For confocal imaging, organoids (10000 cells, in 400 μL full organoid growth medium) were cultured in a Nunc LabTek II chamber slide. Organoids were cultured in complete ADMEM/F12 medium for a total of 3 passages (Figure 6F), or imaged at passage 0 (Figure 6I).

METHOD DETAILS

Prostate isolation and streptavidin-mediated pulldown of avi-tagged proteins

Mice were sacrificed using Schedule 1 methods and prostates rapidly dissected, rinsed in PBS, flash-frozen in N_2(l) and stored at −80°C until use. Tissues were pulverised under continuous flow of N_2(l). For streptavidin-mediated pulldown, typically, 750ul Triton/CHAPS lysis buffer (1% Triton X-100, 0.4% CHAPS, 20 mM Tris-HCl pH 7.4, 150 mM NaCl, 1 mM EDTA, 1 mM EGTA, 2.5 mM $Na_4P_2O_7$, 25 mM NaF, 5 mM Na_3VO_4, 5 mM β-glycerophosphate, 10 μg/mL each of leupeptin, aprotinin, α−pain and pepstatin A, 1 mM PMSF) was added to 50 mg of pulverised tissue to yield an estimated protein concentration of 4 mg/mL. For *Pten*$^{-/-}$ prostate, depending on variations in fluid content of the tissue, a correction factor had to be applied. Lysates were cleared by ultracentrifugation (40000 rpm, 5 min, Beckman Optima Max centrifuge, MLA-130 rotor). An estimated total of 2 mg protein was used per pulldown.

For PLEKHS1-Avi pulldowns followed by immunoblotting with anti-phospho-Y^{258}-PLEKHS1 antibody, prostates were lysed in a modified RIPA buffer (50 mM Tris-HCl pH 7.4, 1% NP-40, 0.5% sodium deoxycholate, 0.1% SDS, 150 mM NaCl, 1 mM EDTA, 1 mM NaF, 2.5 mM $Na_4P_2O_7$, 5 mM Na_3VO_4, 5 mM β-glycerophosphate, 10 μg/mL each of leupeptin, aprotinin, α−pain and pepstatin A, 1 mM PMSF). An estimated total of 6 mg protein was used per pulldown.

Please cite this article in press as: Chessa et al., PLEKHS1 drives PI3Ks and remodels pathway homeostasis in PTEN-null prostate, Molecular Cell (2023), https://doi.org/10.1016/j.molcel.2023.07.015

Broadly, streptavidin-mediated pulldown of Avi-tagged proteins was performed as described in Tsolakos et al.[34] with the following modifications: total time of pulldown was 20 min and beads were washed 4 times post-pulldown prior to elution in 1.5 x SDS sample buffer. For pulldowns followed by immunoblotting with anti-phospho-Y^{258}-PLEKHS1 antibody, total time of pulldown was 1 h and washes were performed with increasing level of stringency: 3 consecutive washes with each of the following: modified RIPA with 0.5% SDS, 0.5 M NaCl or no NaCl.

Biotinylated proteins were eluted from beads by incubation with 1.5 x (2 mg protein) or 2 x (6 mg protein) reducing SDS sample buffer (95°C, 10 min, with 1x vortex after 5 min).

Immunoprecipitation

Pten$^{WT/WT}$ and *Pten*$^{-/-}$ whole prostate lysates were prepared in Triton/CHAPS lysis buffer at an estimated protein concentration of 4 mg/mL as described in 'Prostate isolation and streptavidin-mediated pulldown of avi-tagged proteins'. For p85α IP and control (βCOP), 10 μg antibody was pre-coupled to 50 μL Dynabeads Protein G according to manufacturer's conditions and washed once in Triton/CHAPS pre-IP wash buffer (1% Triton X-100, 0.4% CHAPS, 20 mM Tris-HCl pH 7.4, 150 mM NaCl, 1 mM EDTA, 1 mM EGTA, 2.5 mM $Na_4P_2O_7$, 25 mM NaF). For IRS1 IP (2382, Cell Signaling Technology), 20μL antibody was pre-coupled to 50 μL Dynabeads Protein G, as described above. For phosphotyrosine IP, 4G10 Platinum Anti-Phospho-tyrosine Agarose Conjugate antibody was used (80 μL). Beads were washed 3x in PBS, followed by 3x in pre-IP wash buffer. All lysis and wash steps were performed using ice-cold buffers, on ice.

Lysates were incubated with beads for 90 min, end-on-end (19 rpm) at 4°C. Beads were washed 4x in Triton/CHAPS lysis buffer and bound proteins were eluted in 40 μL 1.5x SDS sample buffer (Dynabeads) or 50 μL 2x SDS sample buffer (Agarose beads), at 95°C, for 10 min, with 1x vortex after 5 min.

Lysates from WT (*PBiCre*$^{+/-}$;*Pik3ca*$^{+/+}$), *Pik3ca*$^{+/HR}$ (*PBiCre*$^{+/-}$;*Pik3ca*$^{+/Lat\text{-}H1047R}$) and *Pten*$^{fl/fl}$ (*PBiCre*$^{+/-}$;*Pten*$^{fl/fl}$) DLP lobes aged 400 days, 370 days and 400 days respectively,[42] as well as control *Pten*$^{WT/WT}$ and *Pten*$^{-/-}$ DLP lobes aged 20 weeks, were prepared in Triton/CHAPS lysis buffer using a mechanical homogeniser (Model Pro 200; Pro Scientific Inc, USA), at an estimated protein concentration of 0.8 mg/mL. The actual protein concentration was determined by BioRad Protein Assay, according to the manufacturer's protocol. A maximum of 0.4 mg protein was used per p85α IP.

WT C57BL/6J and PTEN$^{-/-}$/SHIP2$^{-/-}$ ovary lysates were prepared in Triton/CHAPS lysis buffer at an estimated protein concentration of 4 mg/mL as described in 'Prostate isolation and streptavidin-mediated pulldown of avi-tagged proteins'. Actual protein concentration was determined by BioRad Protein Assay, and 2 mg of total protein was used per IP.

TMT-LC-MS/MS

TMT-6-plex (identification of p85α and -β$^{Avi/Avi}$ interactome), TMT-10-plex and TMT-11-plex Isobaric Label Reagents (analysis of the effect of *in vivo* PI3K inhibition on the p85α-avi interactome; identification of *Plekhs1*$^{Avi/Avi}$ interactome) were from ThermoFisher Scientific. TMT-LC-MS/MS, protein identification and quantification was performed essentially according to Luff et al.[85]

p85$^{Avi/avi}$ interactome analysis

Quantitative MS data (scaled abundances calculated in Proteome Discoverer) was analyzed in RStudio. Abundance values for high-confidence proteins that were identified in at least 3 biological replicates per condition were transformed (sqrt) to meet the assumption of normality for parametric testing. To distinguish specific p85α and/or p85β-interactors from non-specific background, multiple two-sided unpaired *t*-tests (Holm correction) were performed. A stringent significance threshold ($p < 0.01$), and FC of 2 and above, was applied to identify a total of 24 proteins with increased detection above *p85*$^{w/w}$ controls.

Plekhs1$^{Avi/avi}$ interactome analysis

Quantitative MS data (grouped abundances, where each protein is expressed as a proportion of the total signal measured for that protein across all replicates and genotypes, average set to 400, and calculated in Proteome Discoverer) were analyzed in Excel. To distinguish specific PLEKHS1-interactors from non-specific background, ANOVA-based statistical tests were applied to calculate adjusted p value, significant interactors are defined by adjusted p value ≤ 0.05 and FC > 2, for *Plekhs1*$^{Avi/Avi}$ *x Pten*$^{WT/WT}$*: Plekhs1*$^{w/w}$ *x Pten*$^{WT/WT}$ or *Plekhs1*$^{Avi/Avi}$ *x Pten*$^{-/-}$*: Plekhs1*$^{w/w}$ *x Pten*$^{-/-}$. The data for all genotypes is based on n = 3 biological replicates, except *Plekhs1*$^{w/w}$ *x Pten*$^{WT/WT}$, which is based on 2 biological replicates (as a result of the restrictions placed by 11-plex TMT labeling available at the time).

For phosphorylation analysis, phospho S/T/Y were included as additional variable modifications for the database search with Sequest HT, within Proteome Discoverer. The mass spectra of the PLEKHS1 phosphopeptides reported by Sequest were manually interpreted to determine phosphorylation sites.

Label-free, targeted LC-MS protein analyses

Protein complexes from mouse tissues were enriched by antibody pulldowns as described in section 'Immunoprecipitation' and trypsin digested according to Luff et al.[85] Briefly, denatured IP eluates were subjected to SDS-PAGE on 4–15% Mini-PROTEAN TGX Precast Protein Gels (Bio-Rad) until samples entered ~5 mm into the gel. Proteins were visualised with Imperial Protein Stain (ThermoFisher Scientific) and excised.

Samples were reduced and alkylated, washed and dehydrated as described previously.[85] Gel pieces were rehydrated for 20 min at room temperature in 10 ng/μL trypsin/50 mM triethylammonium bicarbonate/0.1% octylglucoside, then digested overnight at 30°C in a total volume of 50 μL.

Targeted LC-MS assays of PI3K subunits and selected interactors used at least three tryptic peptides for each protein: Pik3r1 (TQSSSNPAELR, VLSEIFSPVLFR, NESLAQYNPK), Pik3r2 (ERPEDLELLPGDLLVVSR, VALQALGVADGGER, IQGEYTLTLR), Pik3ca (YEQYLDNLLVR, FGLLLESYCR, LINLTDILK), Pik3cb (TVVSSEISGK, AAELASGDSANVSSR, AFGEDSVGVIFK), Pik3cd (LCDIQPF LPVLR, QPLVEQPEEYALQVNGR, YESYLDCELTK), Plekhs1 (GTGLSLSYYK, DYFLIGHDR, RPVSDPSPFLGLCSIPEGIR, AQTTDD QKGSASLTVVK, ASLPEHLIQK, HQLAESVQR), Irs1 (HHLNNPPPSQVGLTR, GASTLAAPNGHYILSR, SVSAPQQIINPIR), Afap1l2 (DQAEQWLR, VYLDLTPVK, QPEVQESSEPIEPTPR), Pik3ap1 (VSTEAEFSPEDSPSIR, APDLSSGNVSLK, DEELPTLLHFAAK). The analyses were performed on an Orbitrap Eclipse mass spectrometer (Thermo Scientific) with on-line separation by reversed-phase nanoLC. MS1 and scheduled MS2 scans were acquired, and the data analyzed with the aid of Skyline software (Washington University).

GFP-trap pulldown assay

LNCaP cells cultured in 10 cm dishes were transfected 24 h after seeding using Lipofectamine 3000 according to manufacturer's protocol. Cells were harvested 48 h after transfection in Triton/CHAPS lysis buffer (750 μL/dish). For inhibitor treatments, media was replaced and cells pre-treated for 1 h before harvesting. For serum starvation, media was replaced with complete media or starvation media (RPMI-1640 with Pen-Strep, phenol red free) 16 h before harvesting. Crude lysates were vortexed for 10 s and incubated on ice for 10 min with brief vortex at 5 min. Lysates were cleared by centrifugation (>13,000 rpm, 10 min, 4°C, bench centrifuge). ChromoTek GFP-trap beads (30 μL/sample) were pre-washed with lysis buffer (3 × 500 μL). Pulldown was performed by incubating cleared lysates (~1.5 mg) with beads for 1 h with rotation (19 rpm) in cold room. Aliquots of lysates pre- and post-pulldown were reserved for western blotting and BCA assay (pre). Beads were washed with lysis buffer (4 x 1 mL) and bound proteins eluted by boiling for 10 min at 95°C in 2x sample buffer (30 μL/sample). Samples were vortexed briefly before and during (5 min) elution. Pre-/Post-pulldown samples were boiled for 5 min at 95°C in 4x sample buffer. Samples were snap frozen and kept in −80°C for western blots.

Generation of custom-made antibodies

Monoclonal antibodies against the avi-tag were developed by Babraham Bioscience Technologies (BBT)/BRC technology development lab using established methodology[86] where mice were immunised with avi-tag peptide GLNDIFEAQKIEWHE.

Polyclonal antibodies against mouse P-Plekhs1 Y258 were generated by Cambridge Research Biochemicals, where rabbits were immunised with antigen peptide C]-AESN-[pY]-VS-Nle-RS-amide. Harvest bleeds were purified against depletion peptide [C]-AESNYVS-Nle-RS-amide, then the unbound material was purified against antigen.

Polyclonal antibodies against human PLEKHS1 were generated by Cambridge Research Biochemicals. Rabbits were immunised with antigen peptide sequence [C]-APKRSPAIKKSQQKGARE-acid and purified by affinity chromatography on Thiopropyl Sepharose coupled with the antigen.

Western blot

Prostate lysates were prepared as described in section 'prostate isolation and streptavidin-mediated pulldown of avi-tagged proteins'. LNCaP lysates and GFP-trap eluates were prepared as described in section 'GFP-trap pulldown assay'. Organoids were trypsinised, washed once in ice-cold PBS, and pelleted by centrifugation (200g; 5 min; 4°C). Pellets were lysed in Triton/CHAPS lysis buffer at a maximum concentration of $1x10^7$ cells/ml and cleared lysates prepared according to section 'GFP-trap pulldown assay'. Lysates were heated at 95°C for 5 min in 4x SDS sample buffer, amounts of protein as indicated in figure legends were resolved by SDS-PAGE, and transferred to PVDF membranes. Membranes were immunoblotted with the indicated primary antibodies at 4°C overnight, followed by 1–2 h at room temperature. They were then washed in TBS (40 mM Tris/HCl, pH 8.0, 22°C; 0.14 M, NaCl) containing 0.1% v/v Tween 20 (TBST) and incubated with HRP-conjugated secondary antibodies. Membranes were washed in TBST, signals were detected by ECL and quantified using Licor Image Studio Lite v.5.2.

Imaging

Prostates, consisting of anterior, ventral, and dorsolateral lobes (one pair of each lobe), were dissected intact as described previously.[4] 20 μm cryosections were prepared on charged glass slides using a Leica CM1850 cryostat. H&E staining was performed using Mayer's hematoxylin solution and Eosin Y solution, following a standard protocol. Images were acquired using a Zeiss Axio Imager Z2 microscope (EC Plan-Neofluar 10× objective; AxioCam MR Rev3), and automatically stitched with AxioVision software, with shading correction enabled. 12 μm $Pten^{WT/WT}$ and $Pten^{-/-}$ prostate cryosections prepared on charged glass slides were rehydrated in PBS at room temperature for 10 min. Cryosections were washed 1x and incubated for 1 h in block/perm buffer (10% horse serum, 1% fatty acid and endotoxin-free BSA and 0.3% Triton X-100 in PBS). Sections were then labeled with 10 μM Hoechst 33342 (prepared as a 1 mM solution in 200 mL tissue culture-grade dH_2O and 2 mL 95% ethanol) and CK8 antibody (1:500) in block/perm buffer, for 16 h at 4°C. Sections were washed 3x in PBS, followed by incubation with Goat anti-Rabbit IgG Antibody, Alexa Fluor 488. Sections were washed 3x in PBS, mounted in VECTASHIELD (#H-1000) and visualised on an EVOS M5000 cell imaging system, using the 20× objective.

For *Pten*$^{WT/WT}$ and *Pten*$^{-/-}$ DLP organoid imaging, organoids were washed in 300 μL PBS and fixed in 200 μL 4% paraformaldehyde in PBS for 20 min at room temperature. Organoids were washed in PBS and permeabilised with 200 μL per well PBS/1% Triton X-100 (60 min at room temperature). Organoids were then blocked in 200 μL PBS/2% BSA/1% Triton X-100 per well (60 min at room temperature). Organoids were mounted in VECTASHIELD containing DAPI (diluted 1:3 in PBS) and imaged using a Nikon A1-R confocal microscope (Nikon Ti2 body) with a 20x 0.75 NA objective and operated using Nikon Elements software.

For quantification of DLP organoid area, transmitted light images were acquired on the EVOS M5000 microscope, using the 5× objective. Images were imported in Napari, and masks for all organoids generated using the Cellpose plugin (cellpose.org[78]). Masks were corrected manually where necessary.

Measurement of PIP_3

Pulverised prostate tissue (5 mg) was resuspended in initial organic solvent mix (chloroform:methanol 1:2) containing H_20 (organic mix:H_20 in 725:170 ratio). Following this step, 200 μL of the resuspended tissue was mixed with 720 μL of initial organic solvent mix:H_20 with added standards (d6-S/A-PIP_3 (10 ng) and d6-SA-PI(4,5)P_2 (100 ng)). Lipid extraction and quantification of levels of PIP_3 was performed according to previously described methodology.[87] Briefly, samples were washed 2x with 720 μL chloroform. The resulting upper phase was loaded onto a 1 mL Sep-Pak anion-exchange column (Waters) that had been pre-equilibrated in initial organic solvent mix containing H_2O. Samples were passed through the column under low vacuum, and unbound material removed by washing in initial organic solvent mix containing H_2O. Low binding components were eluted with 2 × 1mL washes of column wash buffer (0.5M ammonium acetate, made up in chloroform: methanol: H_2O [10:9:1 (v/v:v)]), followed by washing with 3 × 1 mL initial organic solvent mix containing H_2O. PIP_3 and PIP_2 were eluted with 1 mL acid elution buffer (chloroform: methanol: 10 M HCl [1:2:0.124 (v/v:v)]) followed by 700 μL chloroform. Phases were then split by the addition of 340 μL of H_2O and the lower phase was removed and the lipids within it were derivatized and analyzed by mass spectrometry as previously described[87] except that an additional pre-derivitization wash was included, and the final samples were resuspended in 50μL methanol: H_2O 4:1 v/v. D6-C18:0/C20:4-PIP_3 and -PIP_2. The major acyl-chain species of prostate inositol phospholipids were measured by mass spectrometry, employing neutral loss of derivitized head groups, using a ABSciex QTRAP4000 connected to a Waters Acquity UPLC system, as described previously[87]. PIP_3 response ratios were normalized to PIP_2 response ratio to account for any sample input variability.

LNCaP cells cultured in 6-well plates were transfected 24 h after seeding using Lipofectamine 3000 according to manufacturer's protocol. Cells were harvested 48 h after transfection in 1 M HCl (750 μL/well). Lipid extraction and quantification of levels of PI(3,4,5)P_3 was performed according to previously described methodology.[88]

Organoids cultured in 96-well plates were harvested in 1 M HCl (250 μL/well). Lipid extraction and quantification of levels of PIP_3 was performed according to previously described methodology.[88]

Cloning of Plekhs1 from mouse prostate and generation of bacterial and mammalian expression constructs

Bacterial expression vector pRSET-2x(10His)-MBP-TEV site-mEGFP (hereafter referred to as pRSET-mEGFP) was generated using PCR and multiple insertions between the *Xba*I and *Nde*I sites of pRSET A vector (Thermo Fisher Scientific Waltham, MA, USA). Also, a protein-of-interest (POI)-linker-EGFP sequence was inserted between the *Nde*I (POI start), *Bam*HI (linker) and *Hind*III (EGFP stop) sites using multiple PCR and insertions.

RNA was extracted from whole mouse prostate of a C57BL/6J strain using TRIzol Reagent, according to manufacturer's instructions. First-Strand cDNA synthesis was performed using SuperScript II Reverse Transcriptase in combination with Random Hexamer Primers. 20 μL of resulting cDNA was then used to amplify the isolated PH domain (iPH) of m*Plekhs1* (nucleotide sequence corresponding to amino acids 10–135), or full length m*Plekhs1* (nucleotide sequence corresponding to amino acids 10–459), followed by cloning into pRSET-mEGFP. For cloning of m*Plekhs1* iPH, primers containing engineered restriction sites *Nde*I and *Bam*HI were used. For insertion of full length m*Plekhs1*, the *Bam*HI linker site was modified by PCR to *Kpn*I.

The cloned sequence differs from the canonical m*Plekhs1* sequence (NCBI mouse RefSeq isoform 1), as follows: Serine 77: missing; Amino acids 323–336: missing. Hence, YXXM is Y257 in the cloned sequence (Figures 3B–3E and 5B–5D) and Y258 in the canonical sequence. The peptide coverage from PLEKHS1-Avi pulldowns from *Plekhs1*$^{Avi/Avi}$ x *Pten*$^{WT/WT}$ and *Plekhs1*$^{Avi/Avi}$ x *Pten*$^{-/-}$ prostates demonstrates that the canonical sequence is the most abundant in mouse prostate. For simplicity, we refer to YXXM in the main text as Y258.

The 2x(10 His)MBP-mEGFP (pRSET-mEGFP) empty vector was generated by excision of POI (full length m*Plekhs1*)-linker-EGFP. mEGFP was amplified using primers with engineered restriction sites *Nde*I and *Hind*III, followed by cloning into pRSET-2x(10His)-MBP-TEV site.

For mammalian expression, mouse *Plekhs1* cDNA was amplified from above mentioned pRSET-mEGFP constructs, using primers containing engineered restriction sites *Not*I (forward primer; this primer also carries KOZAK sequence, as well as sequence encoding amino acids 1–9 that are absent in pRSET-mEGFP constructs) and *Xba*I (reverse primer), and cloned into pCMV3-EE.[89] pCMV3-EE-mEGFP was generated by amplification of mEGFP from pRSET-mEGFP, using primers containing engineered restriction sites *Not*I and *Xba*I, followed by insertion into pCMV3-EE.

Site-directed mutagenesis to generate *Plekhs1*-Y257F constructs was performed with the Quikchange Lightning Site-directed Mutagenesis kit (Agilent), according to manufacturer's instructions. Site-directed mutagenesis to generate m*Plekhs1*-ΔPH construct was performed with the Q5 Site-directed Mutagenesis kit (NEB), according to manufacturer's instructions.

Please cite this article in press as: Chessa et al., PLEKHS1 drives PI3Ks and remodels pathway homeostasis in PTEN-null prostate, Molecular Cell (2023), https://doi.org/10.1016/j.molcel.2023.07.015

pLNCX chick src Y527F (Addgene plasmid # 13660) and pLNCX chick src K295R (Addgene plasmid # 13659) was a gift from Joan Brugge. To generate pLNCX, src K295R was excised from pLNCX chick src K295R with *Cla*I after which the vector was re-ligated.

Recombinant protein expression and purification

Mouse PLEKHS1 (10–459) and its isolated PH domain (10–134) were expressed and purified as 2x(10His)-MBP-TEV site-(PLEKHS1 construct)-mEGFP) fusion proteins, along with 2x(10His)-MBP-TEV site-mEGFP alone, in BL21-CodonPlus (DE3)-RIPL Competent Cells. Cells were lysed by probe sonication on ice (0.1 M NaCl, 20 mM TRIS/HCl, 50 mM Na/HPO_4, pH 7.5 with anti-proteases lacking EDTA (HALT) with the addition of TX100 to 1% following sonication) and the lysates were cleared by centrifugation at 30,000 x g for 20 min. The proteins were purified via Co^{2+}-affinity resin (His Pur Cobalt resin), eluted by the addition of 0.25 M imidazole and buffer-exchanged via PD10 columns into 0.2 M NaCl, 1 mM EDTA, 20 mM HEPES/NaOH pH 7.4, at 25°C. For the liposome-based assays, the 2x(10His)-MBP-tag was cleaved by incubation with 6xHis-tagged-Tobacco Etch Virus (TEV)-protease and repurified via Co^{2+} affinity resin. For the PIP strips assays, the proteins were further purified (from the Co^{2+}−column eluates in 0.25 M imidazole) through their MBP tag (MBP-TRAP, equilibrated in 0.2 M NaCl, 1 mM EGTA, 25 mM Na/HPO_4 buffer pH 7.5 and eluted by the addition of 20 mM maltose). All proteins were concentrated (Amicon, 10 kD cut-off) and stored in 50% (w/v) glycerol at −20°C. Their purity and protein concentration (relative to BSA, in the range 0.5–2.0 mg/mL) were assessed by SDS PAGE and Coomassie staining.

Lipid binding assays

To test the lipid binding properties of PLEKSH1 and its iPH domain, protein-lipid overlay experiments were performed using PIP Strips and PIP Array. Strips were blocked for 1 h at RT in 3% (w/v) BSA in TBST. PIP strips and arrays were then incubated for 1 h in the blocking solution containing; 2.5 μg total of purified 2x(10His)-MBP-TEV site-PLEKSH1-mEGFP or 2x(10His)-MBP-TEV site-PLEKSH1-iPH-mEGFP or the control 2x(His10)-MBP-TEV site-mEGFP proteins. After washing, the membranes were incubated for 1 hr with an anti-GFP antibody in blocking buffer followed by washing with blocking buffer and then incubation with HRP goat anti-mouse antibody diluted in blocking buffer. The immunoreactive spots were detected using enhanced chemiluminescence.

For liposome-based sedimentation assays, liposomes were made by sonication of vacuum-dried lipids, in quantities appropriate to give final concentrations in the assay of 150 μM phosphatidylserine, 200 μM phosphatidylcholine, 20 μM phosphatidylethanolamine, 10 μM sphingomyelin with various concentrations of $PI(4,5)P_2$, $PI(3,4)P_2$ or $PI(3,4,5)P_3$ (0.1–4 μM or 0.026–1 mol %), into 0.2 M sucrose containing 20 mM KCl, 20 mM HEPES/NaOH, pH 7.4 at 25°C (the primary sonicated suspensions were diluted 10x into the final assay so that the final extra-liposomal concentration of sucrose was 20 mM). The liposomes were incubated with 120 ng of recombinant protein in assay buffer (total final volume of 150 μL, final concentrations in the assay of; 1 mg/mL BSA, 0.12 M NaCl, 1 mM EGTA, 0.2 mM $CaCl_2$, 1.5 mM $MgCl_2$, 18 mM HEPES/NaOH 7.4, 25°C; with approximately 100 nM free Ca^{2+}) for 3 min at 30°C and then pelleted by centrifugation (40000 rpm, 5 min, Beckman Optima Max centrifuge, MLA-130 rotor). Aliquots of the assays were taken before and after centrifugation, resolved by SDS-PAGE and immunoblotted (1^0 antibody anti-GFP, 2^0 anti-mouse-HRP) to quantify the proportion of the proteins that were sedimented with the sucrose-loaded liposomes.

Flow cytometry

Up to 4 $PTEN^{WT/WT}$ or 2 $PTEN^{-/-}$ prostates were digested in 4 mL Collagenase Type II, at a concentration of 5 mg/mL in ADMEM/F12 mix (ADMEM/F12 supplemented with 10 mM HEPES pH 7.4, 2 mM Glutamax and 1x Penicillin-Streptomycin) for 2 h at 37°C, followed by further digestion in 2 mL TrypLE Express Enzyme with the addition of 10 μM Y-27632 for 15 min at 37°C. The resulting cell suspension was centrifuged (5 min, 350 RCF), resuspended in 1 mL PBS/0.5% BSA, and passed through a 100 μm cell strainer to eliminate clumps of cells. To identify live, nucleated cells the single cell suspension was incubated with 10 μM Hoechst 33342 for 30 min at 37°C. Cells were incubated with CD326/EpCAM-FITC (1:300) and CD49f-PE (1:200) at 4°C, for 45 min. Cells were centrifuged, washed in PBS/0.5% BSA and resuspended in 330 μL sorting buffer (PBS/0.5% BSA, 10 mM HEPES, 2 mM EDTA). 30 μL was reserved as an unsorted sample. 50 μL of TO-PRO3 was added to the remainder and cells were sorted into basal epithelial cells (defined as EpCAM+ CD49f-high), luminal epithelial cells (EpCAM+ CD49f-low) and remainder (EpCAM-) on a BD Influx Cell Sorter. The FITC fluorochrome was detected with the 488 nm laser and 530/30 bandpass filter, and the PE fluorochrome was detected with the 561 nm laser and 585/29 bandpass filter. During sorting, cells were kept at 4°C. Cells were collected in ice-cold PBS, a sample reserved for counting, centrifuged, and immediately flash-frozen in N_2(l).

Cells were sorted on the BD Influx cell sorter using a 100 μm nozzle at 30 psi sheath pressure. 1 drop pure sort mode was used for collection into 1.5 mL tubes.

Bioinformatics analysis

PTEN, IRS1 and *PLEKHS1* OncoPrint data was downloaded from cBioPortal (https://www.cbioportal.org/). *PTEN, PLEKHS1* and *IRS1* mRNA expression RNA-seq data (RNA Seq V2 RSEM) in normal prostate and primary prostate cancers was downloaded from UCSC Xena database (TCGA PanCancer, TCGA Target, GTEx[47]) or cBioPortal (TCGA-PRAD PanCancer).

Grouped comparisons of primary prostate cancer, primary breast cancer and primary uterine endometrioid cancer were performed with cBioPortal using TCGA-PRAD, TCGA-BRCA and TCGA-UCEC PanCancer datasets, respectively.[45,46] Only samples with mRNA (RNA Seq V2 SEM) and protein (RPPA) expression data were selected for analysis. Samples were grouped based on quartiles of *PLEKHS1* mRNA expression (RNA Seq V2 SEM) or *p*-Src Y419 levels (RPPA) and compared for AKT, P-S^{473}-AKT and P-T^{308}-AKT

protein levels (RPPA). For TCGA-PRAD, comparisons for 4E-BP1, P-T^{37}-4E-BP1, P-T^{70}-4E-BP1, RPS6, P-$S^{235, 236}$-RPS6 and P-$S^{240, 244}$-RPS6 were included.

Statistical tests were performed using GraphPad Prism (Kruskal-Wallis) or R (Welch's *t*-test) and are described in figure legends. Boxplots were created using R (ggplot2).

QUANTIFICATION AND STATISTICAL ANALYSIS

General statistical analyses

For pairwise comparisons, two-sided unpaired or paired (depending on experimental design) Student's *t*-tests with Welch correction were used. When multiple comparisons were performed on a given dataset, p values were adjusted with FDR correction. In the particular context of the $p85^{Avi/Avi}$ interactome analysis, where the authors wanted to have a more stringent approach to the selection of interactors, a Holm correction was applied.

When data were baseline-corrected prior to statistical analysis (e.g., Figure 5A: % of $Pten^{-/-}$): multiple two-tailed one-sample *t*-tests were performed (with Holm-Šídák correction).

When more than 2 conditions were compared and two factors were included in the analyses, one-way and 2-way analyses, respectively, were performed followed by Holm-Šídák's multiple comparisons tests.

Where data showed departure from the assumptions for parametric tests, in particular from normality, a transformation was applied (log or sqrt, depending of the departure) prior to the analysis. Significance was determined as $p < 0.05$.

Statistical analyses were performed using GraphPad Prism 9 and R version 4.1.3.